NASA TECHNICAL MEMORANDUM

NASA TM X-64710

PHOTOGRAMMETRY AND PHOTO - INTERPRETATION APPLIED TO ANALYSES OF CLOUD COVER, CLOUD TYPE, AND CLOUD MOTION

By Paul A. Larsen
Aero-Astrodynamics Laboratory

June 1972

NASA

George C. Marshall Space Flight Center
Marshall Space Flight Center, Alabama

MSFC - Form 3190 (Rev June 1971)

TECHNICAL REPORT STANDARD TITLE PAGE

1. REPORT NO.	2. GOVERNMENT ACCESSION NO.	3. RECIPIENT'S CATALOG NO.
TMX-64710		

4. TITLE AND SUBTITLE	5. REPORT DATE
Photogrammetry and Photo - Interpretation Applied to Analyses of Cloud Cover, Cloud Type, and Cloud Motion	June 1972
	6. PERFORMING ORGANIZATION CODE
7. AUTHOR(S) Paul A. Larsen	8. PERFORMING ORGANIZATION REPORT #
9. PERFORMING ORGANIZATION NAME AND ADDRESS George C. Marshall Space Flight Center Marshall Space Flight Center, Alabama 35812	10. WORK UNIT NO.
	11. CONTRACT OR GRANT NO.
	13. TYPE OF REPORT & PERIOD COVERED Technical Memorandum
12. SPONSORING AGENCY NAME AND ADDRESS National Aeronautics and Space Administration Washington, D.C. 20546	14. SPONSORING AGENCY CODE

15. SUPPLEMENTARY NOTES

This work was performed in the Aerospace Environment Division, Aero-Astrodynamics Laboratory, Science and Engineering Directorate.

16. ABSTRACT

A determination was made of the areal extent of terrain obscured by clouds and cloud shadows on a portion of an Apollo 9 photograph at the instant of exposure. This photogrammetrically determined area was then compared to the cloud coverage reported by surface weather observers at approximately the same time and location, as a check on result quality. Stereograms prepared from Apollo 9 vertical photographs, illustrating various percentages of cloud coverage, are presented to help provide a quantitative appreciation of the degradation of terrain photography by clouds and their attendant shadows. A scheme, developed for the U.S. Navy, utilizing pattern recognition techniques for determining cloud motions from sequences of satellite photographs, is summarized. Clouds, turbulence, haze, and solar altitude, four elements of our natural environment which affect aerial photographic missions, are each discussed in terms of their effects on imagery obtained by aerial photography. Data of a type useful to aerial and orbital photographic mission planners, expressing photographic ground coverage in terms of flying height above terrain and camera focal length, for a standard aerial photograph format, are provided. Two oblique orbital photographs taken during the Apollo 9 flight are shown, and photo-interpretations, discussing the cloud types imaged and certain visible geographical features, are provided.

17. KEY WORDS	18. DISTRIBUTION STATEMENT
Photogrammetry Photo-Interpretation Meteorology Cloud Cover Geography	Distribution Codes 14 and 20

19. SECURITY CLASSIF. (of this report)	20. SECURITY CLASSIF. (of this page)	21. NO. OF PAGES	22. PRICE
Unclassified	Unclassified	78	$3.00

MSFC - Form 3292 (May 1969)

TABLE OF CONTENTS

LIST OF ILLUSTRATIONS

LIST OF ILLUSTRATIONS (Concluded)

LIST OF TABLES

SPECIALIZED TERMS

Term	Definition
Altocumulus	A layer or series of patches of rather flattened rounded cloud masses, occurring in a variety of forms, and in some cases, existing at several layers at the same time.
Cirrocumulus	A cloud layer or patch composed of small white flakes or of very small globular masses, usually without noticeable shadows, which are arranged in groups or lines, or more often in ripples resembling those of the sand on the seashore.
Cirrus	Detached high cloud of delicate fibrous appearance, without shading, generally white in color, often of a silky appearance.
Cumulonimbus	A cumulus cloud of very great vertical development (often 4 miles or more deep from base to summit) and comparable horizontal extent, the top of which is composed of ice crystal clouds, its distinguishing characteristic.
Cumulus Congestus	Cumulus clouds which are markedly sprouting and are often of great vertical extent; their bulging upper part frequently resembles a cauliflower.
Cumulus Humilis	Cumulus clouds of only a slight vertical extent; they generally appear flattened.
Datum Scale	The datum scale of a photograph is that scale which would be effective over the entire photograph if all points were projected vertically downward to the datum before being photographed.
Principal Point	The foot of the perpendicular from the interior perspective center of the camera to the plane of the photograph.

SPECIALIZED TERMS (Concluded)

Term	Definition
Pyroclastic Debris	Material ejected from the vent of a volcano, which consists of liquid froth, glass shards, and bits of already solid rock.
Relief Displacement	The displacement of a point on a photograph from its datum photograph position due to its elevation above or below the datum.
Stereogram	A set of photographs or drawings correctly oriented and mounted for stereoscopic viewing.
Tilt Displacement	The displacement of the image of a point on a tilted photograph either outward from or inward towards the isocenter, with respect to its equivalent position on a vertical photograph.

TECHNICAL MEMORANDUM X-

PHOTOGRAMMETRY AND PHOTO - INTERPRETATION APPLIED TO ANALYSES OF CLOUD COVER, CLOUD TYPE, AND CLOUD MOTION

SUMMARY

An Apollo 9 vertical photograph of an area in southeast Arizona was chosen for cloud coverage analysis. A sample terrain area (S.T.A.) on the photograph was isolated, and measurements showed that 24.8 percent of the terrain was obscured by clouds, and that an additional 10.4 percent of the terrain was hidden from the camera's view by shadows from the clouds at the time of exposure. National Weather Service surface observations of sky cover for four locations surrounding the S.T.A. at approximately the same time yielded an average observed value of 27.5 percent cloud cover. The measurement results are favorable but not considered conclusive because of the limited number of trials. Further applications of this cloud cover measurement technique could be considered for testing accuracy of cloud cover prediction models. Insofar as available photographic imagery permits, S.T.A. locations should be chosen which are geographically close to National Weather Service surface observation points.

Stereoscopic examination of vertical photographs of cloud coverages ranging from 15 percent to 70 percent showed that considerable difficulty in conventional photo-interpretation processes is encountered when working with photographs containing more than approximately 25 percent cloud coverage.

Experimental techniques being studied by the Navy for determining cloud motions from satellite photographs, using computerized pattern recognition techniques, may lead to the development of automatic systems for obtaining cloud motion data over much of the earth's surface in real time.

Atmospheric haze has a particularly degrading effect on color aerial photography; air turbulence decreases photographic image definition quality because of image motion resulting from aircraft bounce; sun angles lower than 30 degrees cause objectionably long shadows to be recorded on the imagery; and cloud cover greater than 10 percent normally will prevent a planned aerial photographic mission from occurring.

For a given flying height, an increase in camera focal length will decrease the resultant ground coverage recorded on the film format; assuming a constant focal length, an increase in flying height will result in an increase in ground coverage.

When conducting cloud photo-interpretation analyses on oblique orbital photographs, one must exercise care in judging relative sizes or depths of cloud structures in the imagery because of the two types of scale variation inherent in high and low oblique photographs. Stereoscopic examination of sequential vertical orbital and aerial cloud photographs appears more attractive than does oblique photography, when one is interested in judging relative cloud formation height and cloud type.

I. INTRODUCTION

Cloud amounts, cloud types, and cloud motions have been observed and studied by meteorologists for a long time. Weather phenomena are quite often associated with various types of cloud formations, in that each cloud type is indicative of the atmospheric process in operation at the time of observation. Cloud observations, coupled with weather reports and forecasts, serve as a check on development of weather conditions. Clouds are a suspension of many water droplets and ice crystals in the air, and are formed by transformation of some of the water vapor in the atmosphere to a solid or liquid state. It has been estimated that about 50 percent of the earth's surface is cloud covered at any time [1, p. 32].

Clouds are definitely a deciding factor relative to whether good quality orbital or aerial photographic imagery can be obtained. Accordingly, this report was prepared to show by engineering example how varying amounts of cloud coverage detract from the value of photographic imagery from which some type of "earth surface" information is intended to be interpreted; for example, the imagery to be obtained by Skylab experiment S-190, the Multispectral Photographic Facility, and the imagery to be obtained by the ERTS-A Return Beam Vidicon Camera System. The report also endeavors to show that, by basic photogrammetric techniques, one can readily determine the amount of terrain obscured by cloud coverage, as well as terrain obscured by cloud shadow coverage, on a vertical orbital photograph. This photogrammetric technique is verified by comparing its results with those data obtained by surface weather observers, to confirm that it yields reasonably accurate results.

To aid those charged with the responsibility of planning aerial and orbital photographic missions, a section of the report tells how clouds and other natural environmental factors, can affect such mission planning. Also, to assist mission planners, parametric data relating photographic ground coverage to flying height and camera focal length are provided.

The use of oblique orbital photographs in studying cloud formations is illustrated by two Apollo 9 photographs which were taken over southern Mexico and eastern Florida on March 9, 1969, and March 10, 1969, respectively. The photographic scale of an oblique photograph is discussed, and a few cautionary comments pertaining to scale definition in oblique photography, are made.

A summary describing an interesting Navy research study addressing the problem of extracting real time information describing direction and speed of cloud motions, from sequential cloud photographs, has been included. Cloud photographs used in this study for the Navy were obtained by geosynchronous satellites ATS I and ATS III. The approach described may prove worthy of consideration for real time mission planning in future earth survey missions which will follow today's Skylab and ERTS-A and B programs.

The Apollo 9 photograph used in the study of terrain obscuration by clouds and cloud shadows, was taken on March 9, 1969, of an area bounded by Willcox, Arizona; Douglas, Arizona; and Lordsburg, New Mexico. The Apollo 9 photographs used in the stereographic analyses of varying percentages of cloud coverage, were taken on March 8, 9, and 10, 1969, over these four locations: (1) The California sea-coast between Los Angeles and San Diego; (2) The Salton Sea and areas to its west in southern California; (3) The vicinity of Tucson, Arizona; and (4) portions of Querétaro and Hidalgo Provinces, north-west of Mexico City, Mexico. The Apollo 9 oblique photographs, interpreted for cloud formation and geographical information content, taken March 9 and 10, 1969, show part of the southern sea-coast of Mexico and the eastern coastline of Florida. Credit for taking the Apollo 9 photographs used in this report goes to Astronauts James A. McDivitt, Russell L. Schweickart, and David R. Scott.

It is pointed out that, at this time, considerable research efforts are being put forth for the purpose of automating the photo-interpretation process by the use of combinations of advanced photogrammetric equipment, optical devices, and various types of computers. This is as it should be, since the next logical step is to provide machine interpretation of photographic imagery. To fully utilize the voluminous amount of earth imagery to be obtained from the Skylab and ERTS programs, the engineering and scientific communities must be prepared logistically to handle it. Hopefully, this will be the case. Nonethe less, it is the opinion of this author that even after the advent of automated photo-interpretation equipment, these more exotic devices will not supplant the efforts of engineers using one photograph or a few sequential photographs for the purposes of making measurements or analyses to suit his or his employer's own specific needs. In fact, the amount of professional activity in this area will probably increase because a greater selection of orbital platform acquired imagery, e.g. Skylab and ERTS, as well as aircraft underflight imagery, will be available from which to choose for specific applications and needs. It is hoped, accordingly, that this report serves to illustrate how available orbital imagery can be put to work on basic engineering applications, and that much useful information can be gleaned from the imagery without necessarily resorting to exotic automated techniques.

The author wishes to express his sincere appreciation to the following government and private organizations which provided the photographs, maps, and illustrations used in this work discussed herein: The Photographic Division of Marshall Space Flight Center; The Earth Resources Research Data Facility of Manned Spacecraft Center; The Naval Weather Research Facility of the Naval Air Systems Command; The American Society of Photogrammetry; The Department of the Interior; and the Rand McNally Company.

Special thanks are extended to the following individuals who helped the author in various ways to complete this report; Mrs. Evelyn Carter, Mrs. Sarah Hightower, and Mr. S. Clark Brown of Marshall Space Flight Center; Mr. Edward O. Zeitler and Mr. Merritt J. Bender of Manned Spacecraft Center; Mrs. Theresa M. Sousa of the Department of Interior; and Mr. F. E. Bittner of the Naval Weather Research Facility.

II. PHOTOGRAMMETRIC DETERMINATION OF TERRAIN OBSCURATION BY CLOUDS AND CLOUD SHADOWS

The Apollo IX photograph (No. AS 9-26A-3753A), as shown in Figure 1 was made with a Hasselblad camera, using SO-180 Ektachrome infrared film and a Photar 15 filter. This photograph, whose principle point is located at 32° 02'N and 109° 21'W, provides coverage of a 5480 square mile (14 376 km^2), area in southeast Arizona. The photograph was taken at 19:37 Greenwich Mean Time (12:37 p.m. Mountain Standard Time), from an altitude of 103 nautical miles (191 km), on March 9, 1969. The film/filter transmittance response was 0.510-0.890 micrometers [2]. Physiographic features in the photograph are the Chiricahua Mountains and Coronado National Forest (dark tear drop shaped area to the right of center), and Willcox Playa (light triangular shaped area to the left of center). The average scale of the photograph, expressed as a representative fraction, is $\frac{1}{538\,000}$.

The object of this analysis was to select an Apollo photograph which contained a clearly visible and well defined cloud pattern structure, choose a Sample Terrain Area (S.T.A.), and then measure (1) the portion of the S.T.A. which was obscured from the camera's view by the clouds, and (2) the portion of the S.T.A. which was obscured from the camera's view by the shadows of the clouds.

After reviewing the "Apollo 9 Photographic Plotting and Index Report" [2], photograph AS 9-26A-3753A was selected as a good choice for this analysis, based upon the selection of catalogued Apollo 9 photographs which contained cloud formations.

Before describing the procedures used to measure the various elements of imagery area on the photograph, several important factors relating to the verticality of the camera's optical axis at time of exposure, and the reasons for selecting the area shown in Figure 1 should be discussed. According to basic fundamentals of photogrammetry, one must exercise caution in making measurements of any kind on so called "vertical" photographs because of the effects of relief displacement, tilt displacement, and scale variation.

Compared with an equivalent vertical photograph, the relief displacement on a tilted photograph will be less on the half of the photograph upward from the axis of tilt, greater on the downward half of the photograph, and identical for

MARCH 9, 1969

ORBITAL ALTITUDE, H

= 103 n. mi.

(191 km)

TIME OF EXPOSURE, t

= 19:37 G.M.T.

= 12:37 M.S.T.

PHOTOGRAPHIC SCALE, S

= 1/538,032

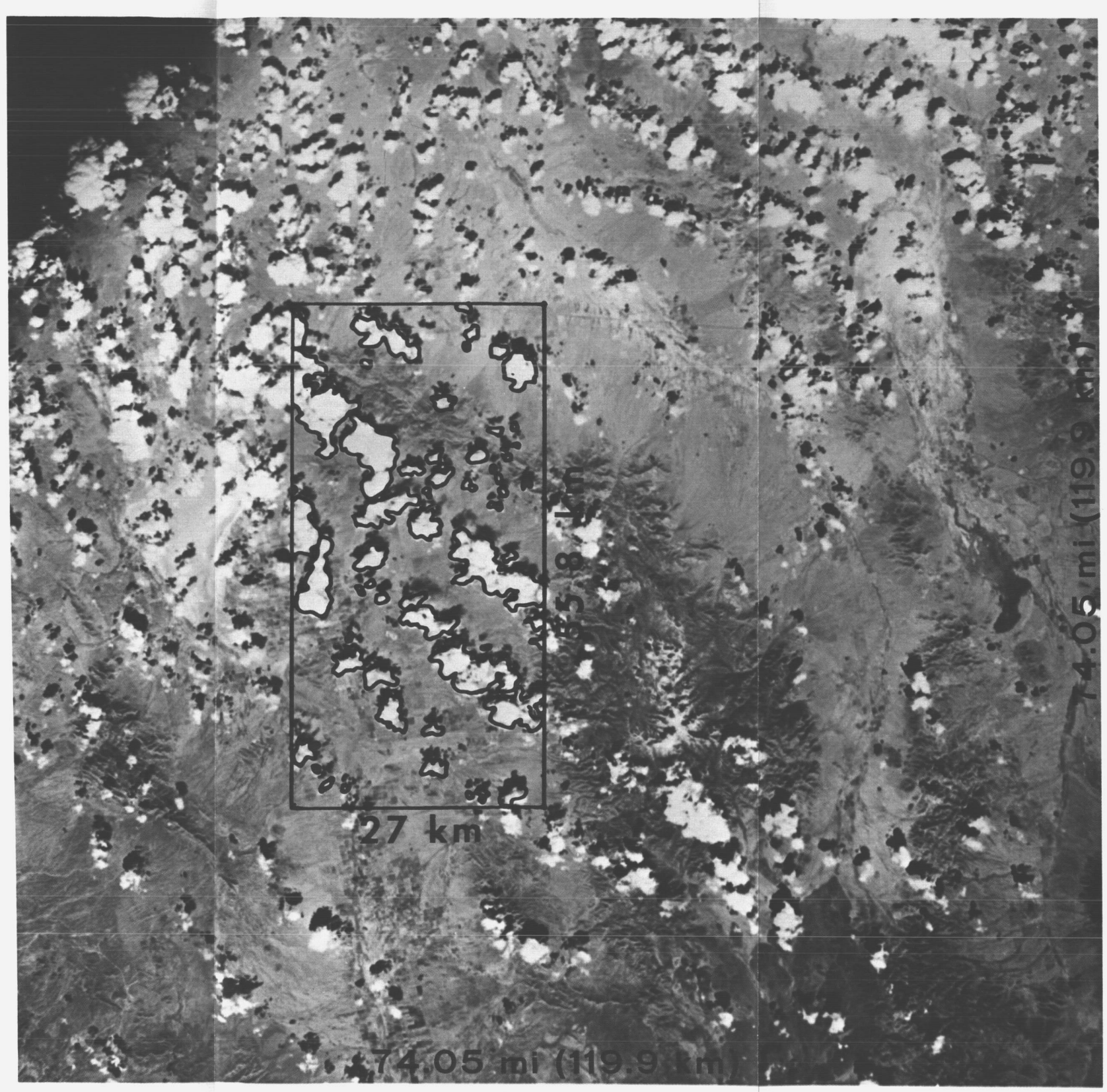

FIG. 1. APOLLO 9 PHOTOGRAPH AS 9-26A-3753A

points lying on the axis of tilt. On a vertical photograph, relief displacement takes place radially on a line from the principal point; for a constant elevation, relief diaplacement of a point increases with the distance from the principal point. Tilt displacement of a point on the upward half of a tilted photograph is inward toward the isocenter, and tilt displacement for a point located on the downward half of a tilted photograph is outward from the isocenter. Also, as the image elevations in different areas of the photograph vary, the photographic scale varies as well.

Because of these variable factors, the S.T.A. outlined in black in Figure 1 was chosen since it was reasonably close to the photograph's principal point, thereby minimizing the effects of relief and tilt displacement on the imagery of interest. Displacements of the cloud shadow images from the cloud images appeared reasonably similar from one cloud to the next in the S.T.A., indicating that the elevations of the cloud tops of the majority of the clouds were roughly identical. In addition, the clouds and shadows themselves were clear and well defined, thereby facilitating measurements of their areas. Since the mission constraint for photograph AS 9-26A-3753A and the other photographs of the SO-65 experiment required that the optical axis be no more than ± 5 deg off nadir (within ± 5 deg from vertical), it is safe to assume that this photograph's tilt angle is within that tolerance.

The first step in preparing the photograph for area measurement was to tape it down to a portable light table. The sample terrain area was then outlined on the photograph. A piece of transparent tracing paper was secured to the photograph, and the cloud images were carefully outlined using a fine pen. After all of the cloud images were outlined, the tracing paper was removed from the photograph, and a transparent mylar overlay of the "cloud only" picture was produced on a thermo-fax machine. The tracing paper was then carefully repositioned on the photograph, and the outlines of the cloud shadows were added to the outlines of the clouds. The tracing paper was removed again, and another transparent mylar overlay which showed "the clouds and the cloud shadows" was produced on a thermo-fax machine. A reproduction of the two transparent overlays is shown in Figure 2.

The next step was to reproduce the "clouds only" outlines and the "clouds and cloud shadows" outlines on white sheets of paper by means of a Xerox machine from the two transparent overlays. From these reproductions colored drawings were prepared showing (a) Clouds Only, (b) Shadows Only, and (c) Clouds and Shadows. These colored drawings, arranged adjacent to one another for ease of comparison, are shown in Figure 3. To measure the areas of "clouds only" and "shadows only" the colored drawings showing

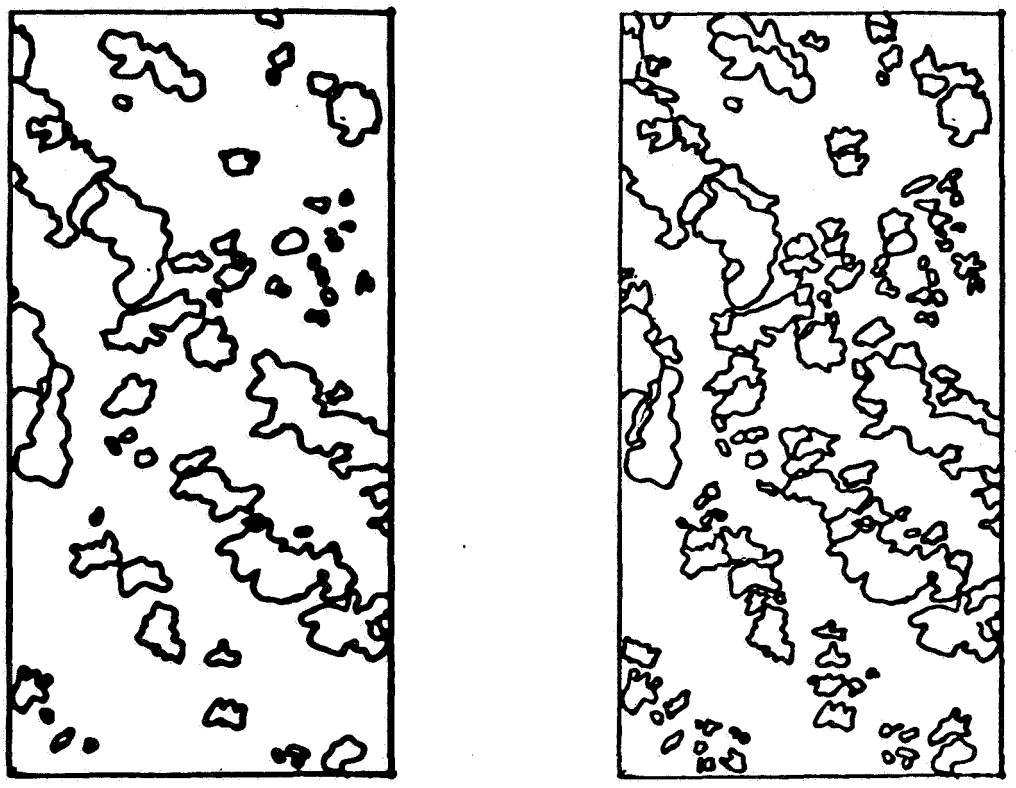

Clouds Only

Clouds and
Cloud Shadows

FIG. 2. REPRODUCTION OF TRANSPARENT OVERLAYS FOR SAMPLE TERRAIN AREA

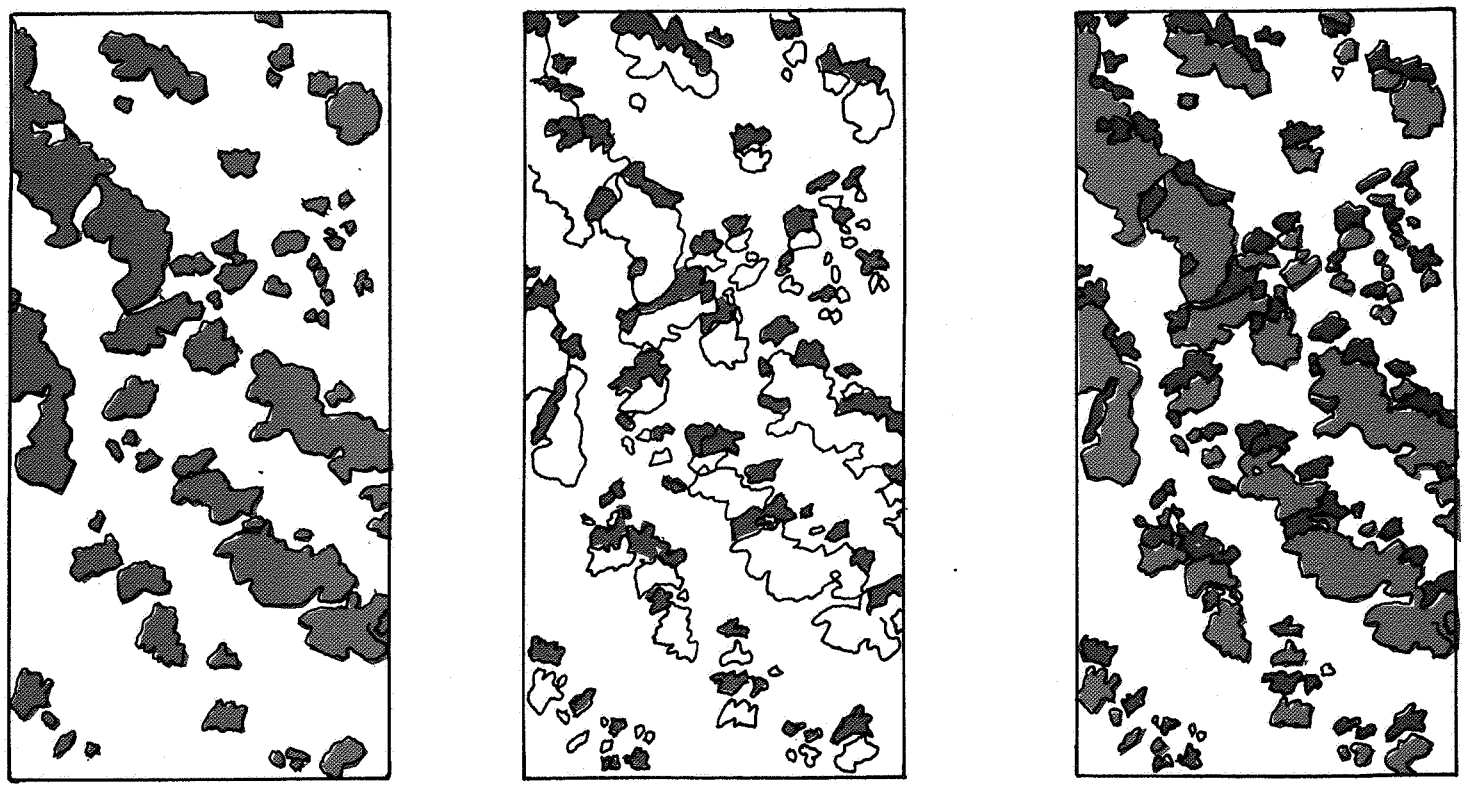

FIG. 3. GRAPHICAL COMPARISON OF THE ELEMENTS OF TERRAIN OBSCURATION

"clouds only" and "shadows only" were first fastened onto the portable light table mentioned earlier. A grid sheet, made from 10 × 10 to the cm graph paper, was placed over the colored drawings, and the 1 mm × 1 mm squares of the 10 × 10 to the cm graph paper were marked to record "cloud only" elemental areas and "shadows only" elemental areas, respectively. A reproduction of this grid sheet is shown in Figure 4.

The marked elements in each horizontal row of the "clouds only" and "shadows only" grid sheets were then counted, and the row results were added, for each grid sheet.

The S.T.A. measured on photograph 3753A (Fig. 1) was 5050 mm^2. The percentage of the S.T.A. obscured by clouds only, as viewed by the camera from orbital altitude was calculated as follows:

$$\frac{1254\ mm^2}{5050\ mm^2} \times 100\% = 24.8\%$$

since 1254 mm^2 of cloud area were measured by the "clouds only" grid sheet shown in Figure 4. The percentage of S.T.A. obscured by cloud shadows only, as viewed by the camera from orbital altitude was calculated as follows:

$$\frac{525\ mm^2}{5050\ mm^2} \times 100\% = 10.4\%$$

since 525 mm^2 of shadow area was measured by the "shadows only" grid sheet shown in Figure 4. The percentage of sample terrain area obscured by clouds and cloud shadows, as viewed by the camera from orbital altitude, was:

$$24.8\% + 10.4\% = 35.2\%$$

In terms of the Earth Resources Technology Satellite "ERTS-A", and the Earth Resources Experiment Package "EREP" to be flown on Skylab, this figure of 35.2 percent is of some interest. As mentioned earlier in this report, the time of exposure of this photograph was 19:37 G.m.t. or 12:37 Mountain Standard time, and the sun elevation at that time was 55 deg. It is quite likely

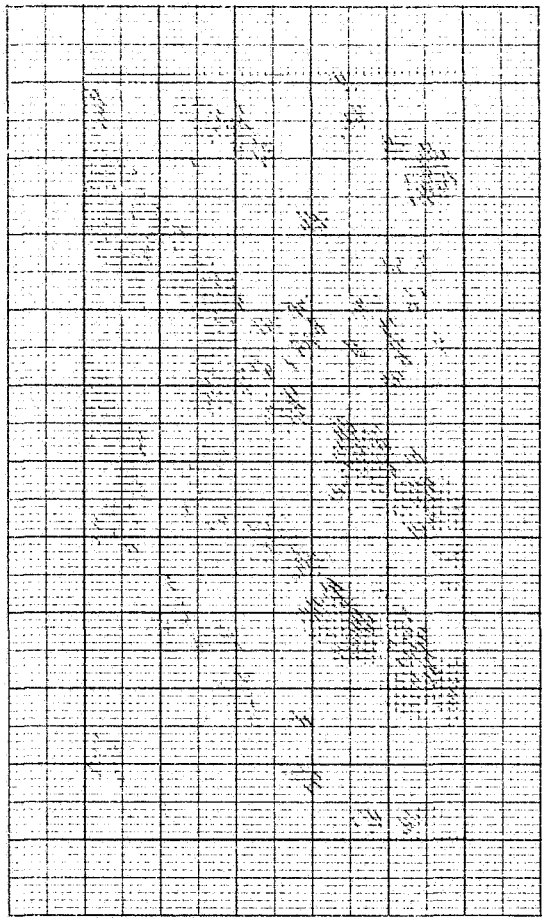

Clouds Only

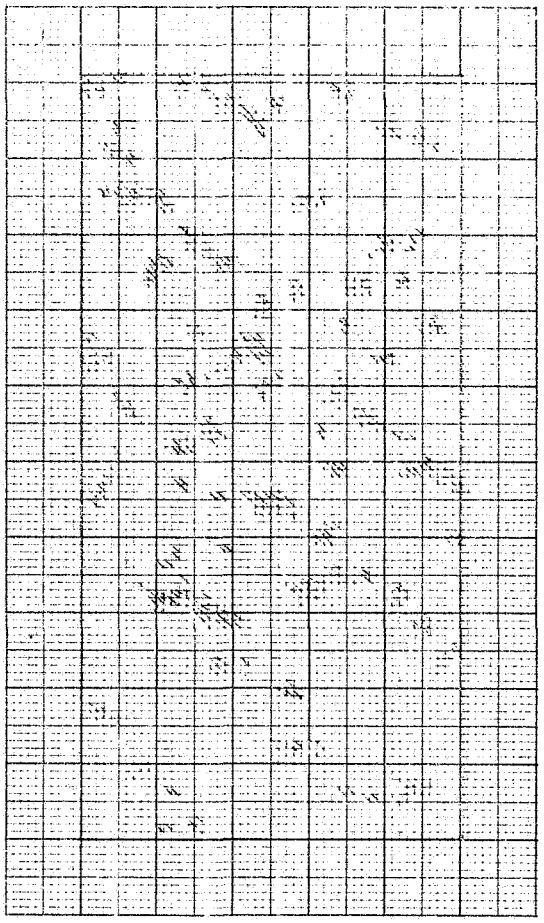

Shadows Only

FIG. 4. REPRODUCTION OF GRID SHEET USED IN MEASURING CLOUD AREA AND SHADOW AREA

that remote sensing planned for the ERTS-A and EREP missions in the visible range (photography) will be planned to take place for the most part around noon ± 2 hours local time, at least for the vertical photography. Accordingly, when existing cloud coverage is a consideration as to whether imagery in the visible range should be taken of a geographical area at a particular time of an orbit, the degree of cloud coverage over an area should not be divorced from the attendant amount of terrain which is obscured by the shadows resulting from the clouds. In addition, it must be kept in mind that the amount of shadow produced by the cloud increases as the sun elevation angle decreases.

III. PHOTOGRAMMETRIC DETERMINATIONS OF CLOUD COVERAGE COMPARED TO CLOUD COVERAGE REPORTED BY SURFACE WEATHER OBSERVERS

After completing the photogrammetric analysis of terrain obscuration by clouds and cloud shadows, as measured on a sample terrain area of the Apollo 9 photograph, the next step was to try to obtain cloud coverage observations from the National Weather Service for geographical areas in the vicinity of the sample terrain area as shown in Figure 1. It was believed that a comparison of the cloud coverage revealed by the camera from 103 nautical miles (191 km) altitude with the coverage observed by ground-based weather observers would be of interest.

U.S.G.S. map sheets of Douglas, Arizona, and Silver City, New Mexico, at a scale of 1:250 000 proved to be useful geographical references in this study. Figure 5 shows the U.S.G.S. maps joined together about 2/5 of the way down from the top of the picture at a reduced scale. A transparent overlay was superimposed over the map and the S.T.A. rectangle was marked upon it, to correspond with the S.T.A. rectangle as shown on the photograph in Figure 1.

Upon studying this map, it was concluded that the three most desirable towns, from a geographical viewpoint, with respect to proximity to the S.T.A., for obtaining comparative cloud cover observations for March 9, 1969, at 12:37 Mountain Standard Time, would be Douglas, Arizona, to the south, Willcox, Arizona, to the west, and Lordsburg, New Mexico, to the east.

NOAA's National Climatic Center at Asheville, North Carolina, was queried about the availability of surface weather observations for those three locations. National Climatic Center was able to furnish data for Douglas, Arizona, but not Willcox, Arizona, or Lordsburg, New Mexico. However, in addition to data from Douglas, Arizona, they also furnished surface weather observations from Tucson, Arizona to the west of the S.T.A.; Ft. Huachuca, Arizona to the southwest; Deming, New Mexico to the east, and Silver City, New Mexico to the north-east. These locations can be seen on Figure 6, a map of the areas under consideration.

Meteorologists of the National Weather Service record surface weather observations on a standard form called WBAN Form 10, normally referred to as WBANs (pronounced "we-bans"). The information which the National Climatic Center furnished in response to our request was in the form of WBANs. A host of other data such as pressures, temperatures, dew

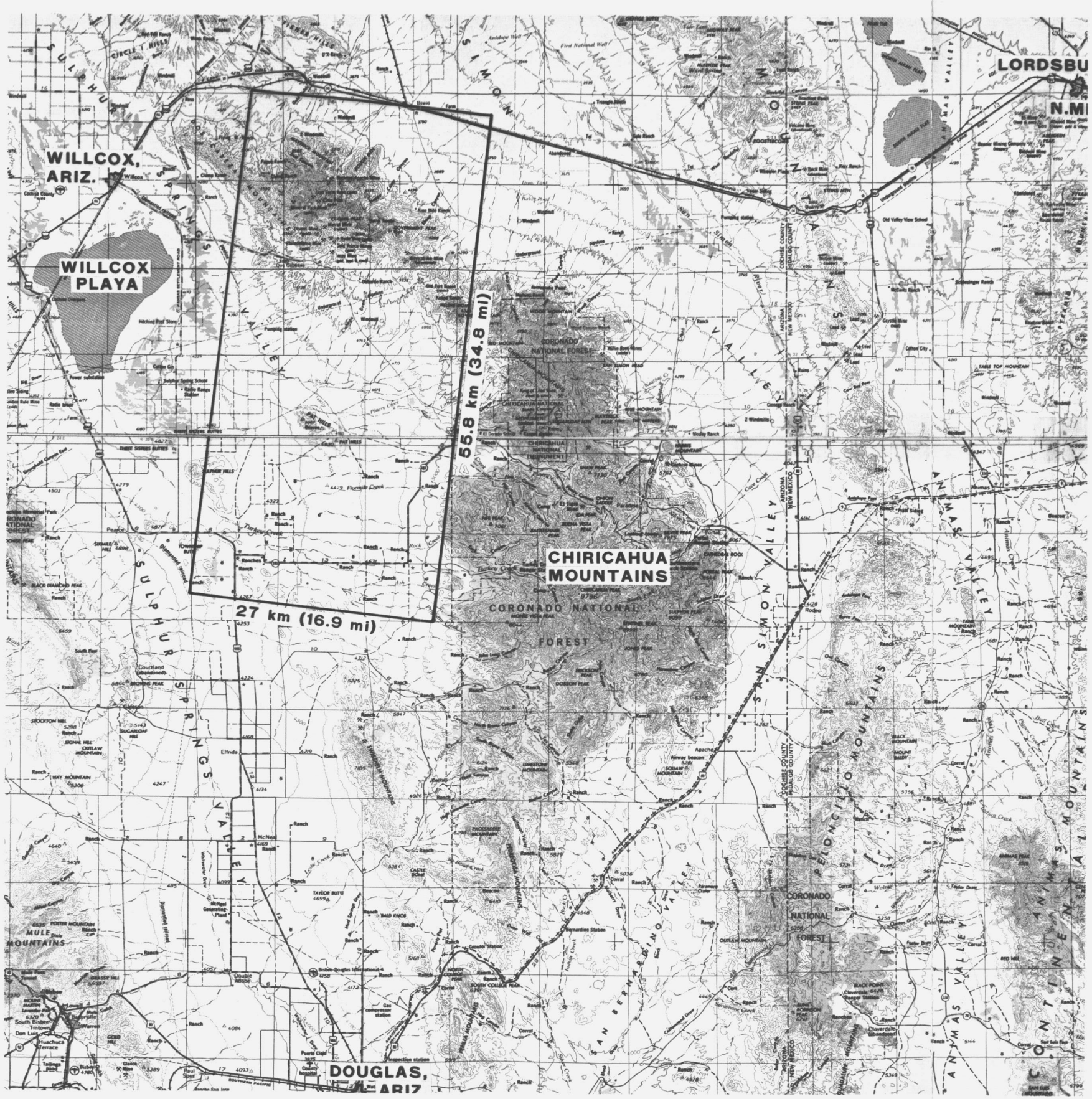

FIG. 5. USGS MAP SHEETS OF DOUGLAS, ARIZ., AND SILVER CITY, N. MEX., SHOWING SAMPLE TERRAIN AREA

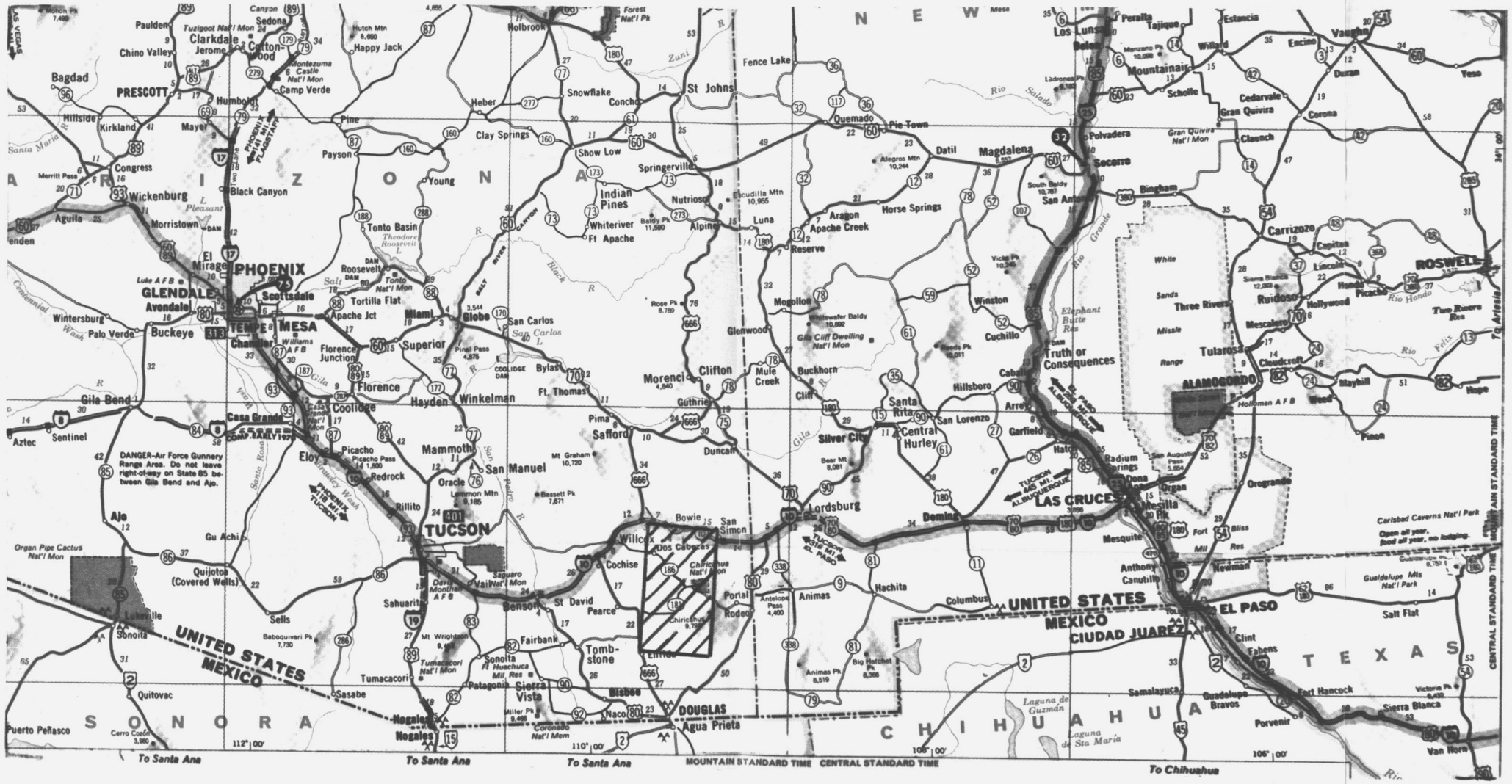

*© *RAND McNALLY & COMPANY, R.L. 72-Y-70*

FIG. 6.* MAP SHOWING SEVERAL LOCATIONS FOR WHICH SURFACE WEATHER OBSERVATIONS WERE OBTAINED

points, station pressures, relative humidity, etc., are included on the WBANs, in addition to clouds and obscuring phenomena, visibility, and sky and ceiling information. The former items are not considered of vital importance to this investigation, and they are not mentioned further. The latter items dealing with clouds, visibility, etc. are, however, of some significance to this investigation, and will be considered in some detail.

The cloud related parameters have been extracted from the WBANs for 12:58 local time on March 9, 1969, for Tucson, Arizona; Ft. Huachuca, Arizona; Douglas, Arizona; and Deming, New Mexico, and have been summarized in Table 1. The next section includes interpretations of the surface weather observations for each of the above mentioned locations in the vicinity of the S.T.A.

Cloud Cover Interpretations of National Weather Service Surface Weather Observations

Tucson, Arizona

Surface weather observation records showed that cloud bases existed at 7000 feet (2134 m) above the station; also, scattered clouds were reported as covering about 50 percent of the sky. Surface visibility was 60 statute miles (96.6 km); wind was blowing from the southwest at 14 knots (26 km/hr); total sky coverage of 50 percent consisted of clouds only (no smoke or haze); and the clouds were opaque.

Ft. Huachuca, Arizona

Surface weather observation records showed cloud bases to be at 5500 feet (1676 m) above the station; clouds were scattered; wind was blowing out of the south-west at 20 knots (37.1 km/hr); total sky cover was 20 percent, clouds were opaque; and surface visibility was 60 statute miles (96.6 km).

Douglas, Arizona

Surface weather observation records showed cloud bases of a scattered cloud formation to be at 5000 feet (1524 m); another scattered layer was located above 20 000 feet (6096 m); surface visibility was 30 statute miles (48.3 km); the wind was blowing out of the south-south-east at 16 knots (30 km/hr); some smoke was visible to the south; and a total opaque sky cover of 30 percent was estimated by the surface weather observers.

TABLE 1. CLOUD-RELATED PARAMETERS RECORDED BY SURFACE WEATHER OBSERVERS FOR FOUR LOCATIONS ON MARCH 9, 1969

Location	Time (Local = m. s. t.)	Type	Sky and Ceiling	Visibility-Surface [statute miles (km)]	Wind Direction	Wind Speed [knots (km/hr)]	Total Opaque Sky Cover
Tuscon, Arizona	12:58	R	70 ⊕	60 (97)	24	14 (26)	5
Ft. Huachuca, Arizona	12:58	R	55 ⊕	60 (97)	22	20 (37)	2
Douglas, Arizona	12:59	R	50 ⊕/⊕	30 (48)	21	16 (30)	3
Deming, New Mexico	12:59	R	70 ⊕	50 (81)	17	08 (15)	1

Deming, New Mexico

Surface weather observation records showed cloud bases to be at 7000 feet (2134 m) above the station; clouds were scattered; surface visibility was 50 statute miles (80.5 km), and windspeed was 8 knots (14.8 km/hr) out of the south-southeast. Total opaque sky cover of 10 percent was reported.

It is pointed out that although Apollo 9 photograph 3753A was taken at 12:37 local time, the ground surface observations used for comparisons were made at 12:58 local time for Tuscon and Ft. Huachuca, (21 minutes later), and at 12:59 local time for Douglas and Deming, (22 minutes later), since these observations were closest in time to the instant of exposure of the photograph. Furthermore, when a meteorologist makes a surface weather observation to record sky and ceiling and cloud cover phenomena, he looks above and all around him to make his estimates.

Even though there was a small time difference between ground observation and instant of photograph's exposure, and admittedly the ground observation method is somewhat of a "judgement based on experience" procedure, the cloud cover observed in the S.T.A. by the camera and the total opaque cloud cover observed by the meteorologists at the four previously mentioned locations were in reasonable agreement. If one takes an arithmetic average of the total opaque cloud cover of the four locations $\left(\frac{5+2+3+1}{4}\right)$, a figure of 2.75 "tenths" or 27.5 percent is obtained. As mentioned earlier in section II, the cloud coverage measured in the S.T.A. was 24.8 percent. One might ask "What is the value of making cloud observations from orbit if such good estimates can be made by surface based weather observers?" One important reason for orbital cloud observations is that a greater number of geographical areas of the country can be covered by this orbital or synoptic view, some of which may not have National Weather Service or F.A.A. (Federal Aviation Administration) surface weather observations sites.

IV. STEREOGRAMS ILLUSTRATING VARIOUS PERCENTAGES OF CLOUD COVERAGE

Shown in this section are four stereograms depicting various percentages of cloud coverage over several geographical locations in western United States, and Mexico.

The amount of cloud coverage shown in the component photographs of the stereograms, ranges from 15 percent on Apollo 9 photograph no. AS 9-26-3731 through 70 percent on Apollo 9 photograph no. AS 9-26-3764. "The percent cloud cover was estimated by overlaying each photograph with a clear film grid which subdivided the image area into 100 squares. A visual estimation was then made as to the percent of the image area covered by clouds." (quoted from Reference 2). These cloud cover estimates were made in the Mapping Sciences Laboratory of the Manned Spacecraft Center, Houston, Texas. One photograph from each stereogram was chosen for inclusion at a somewhat larger scale, adjacent to the stereogram, for the benefit of readers not having stereoscopic vision or for those not having access to a small stereoscope. The small-scale photographs used in constructing the stereograms were prepared from exposures made on 3400 Panatomic -X Film and the larger scale colored photographs were prepared from exposures made on S-180 Ektachrome Infrared Film. All photographs in this section were results of the SO-65 multispectral experiment flown on Apollo 9. (The stereograms and photographs are presented as Figures 7 through 14).

Readers of this report who have access to a pocket stereoscope for viewing the stereograms will find that the cloud formations and certain prominent terrain features lend themselves well to stereoscopic viewing. Of course, as can be seen in the stereograms and in the larger scale infrared photographs, this observability of terrain features decreases considerably as the percentage of cloud coverage increases. This fact highlights the purpose of showing these photographs, which is to give a viewer an impression of how even the smaller amounts of cloud coverage detract from the value of earth imagery taken from space, if it is to be used for photogrammetric or photo-interpretation purposes in connection with, for example, earth resources applications.

The photograph number is specified above each photograph in the stereograms and the percentage of cloud coverage is shown with each photograph. Brief comments concerning the meteorology and geography depicted within each stereogram are provided. Table 2 lists the principal point location, sun elevation, altitude of the camera, and other information pertinent to each photograph. These data were extracted from Reference 2.

Datum scales, expressed as ratios, are provided for each stereogram and infra-red color enlargement. The datum scale calculations were based upon a focal length of 80 mm and the camera altitudes at the time of each exposure, as given in Reference 2.

TABLE 2. APOLLO 9 SO-65 MULTISPECTRAL PHOTOGRAPH DATA

Photograph Frame Number	Date of Exposure	Time of Exposure (G.m.t.)	Principal Point Location				Camera Altitude		Sun Elevation (deg)	Percent Cloud Coverage
			Latitude		Longitude					
			deg	min	deg	min	n. mi.	km		
AS-9-26-3731	3-9-69	1802	33	05N	118	33W	106	196.4	45	15
AS-9-26-3732	3-9-69	1802	33	09N	117	50W	106	196.4	45	20
AS-9-26-3747	3-9-69	1936	33	09N	116	14W	103	190.9	45	35
AS-9-26-3748	3-9-69	1936	33	03N	115	45W	103	190.9	45	30
AS-9-26-3707	3-8-69	2001	32	40N	111	20W	105	194.6	53	45
AS-9-26-3708	3-8-69	2001	32	35N	111	03W	105	194.6	53	55
AS-9-26-3764	3-10-69	2052	20	46N	100	15W	104	192.7	55	70
AS-9-26-3765	3-10-69	2052	20	33N	99	38W	104	192.7	55	60

AS 9-26-3731

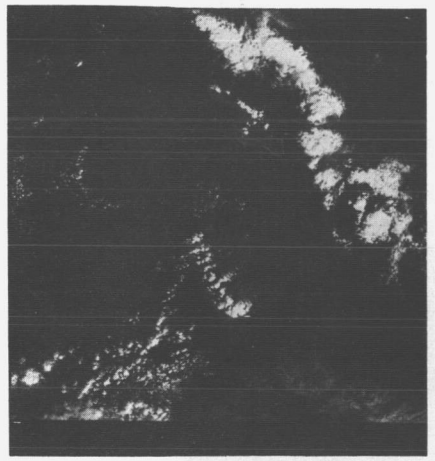

15% Cloud Coverage

AS 9-26-3732

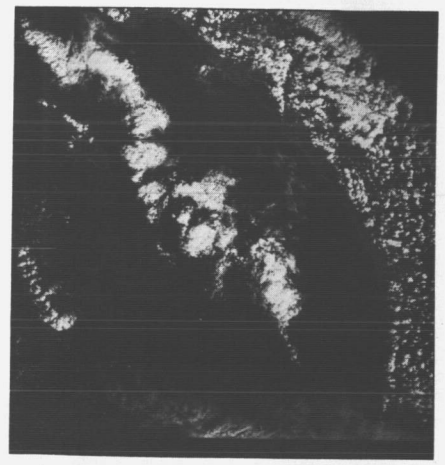

20% Cloud Coverage

Scale 1:2,456,000

FIG. 7. STEREOGRAM 3731/3732

Comments for Stereogram 3731/3732

Meteorology: Cloud forms visible in stereogram are: Cirrocumulus, Cumulus Congestus, Cumulonimbus, and Cumulus Humilis. An especially prominent Cumulonimbus formation is located to right of center of stereogram's overlap area.

Geography: San Clemente and Santa Catalina Islands, capped by cloud formations are clearly visible. Sediment outflows into the Pacific can be seen from several of the coastal cities south of Los Angeles, mid-way to San Diego, visible in the lower right corner of photograph 3732 A. San Pedro Channel, to the east of Santa Catalina, marks the beginning of the cumulus lane, which extends diagonally to the south-east and the waters off La Jolla and Pacific Beach, just north of San Diego.

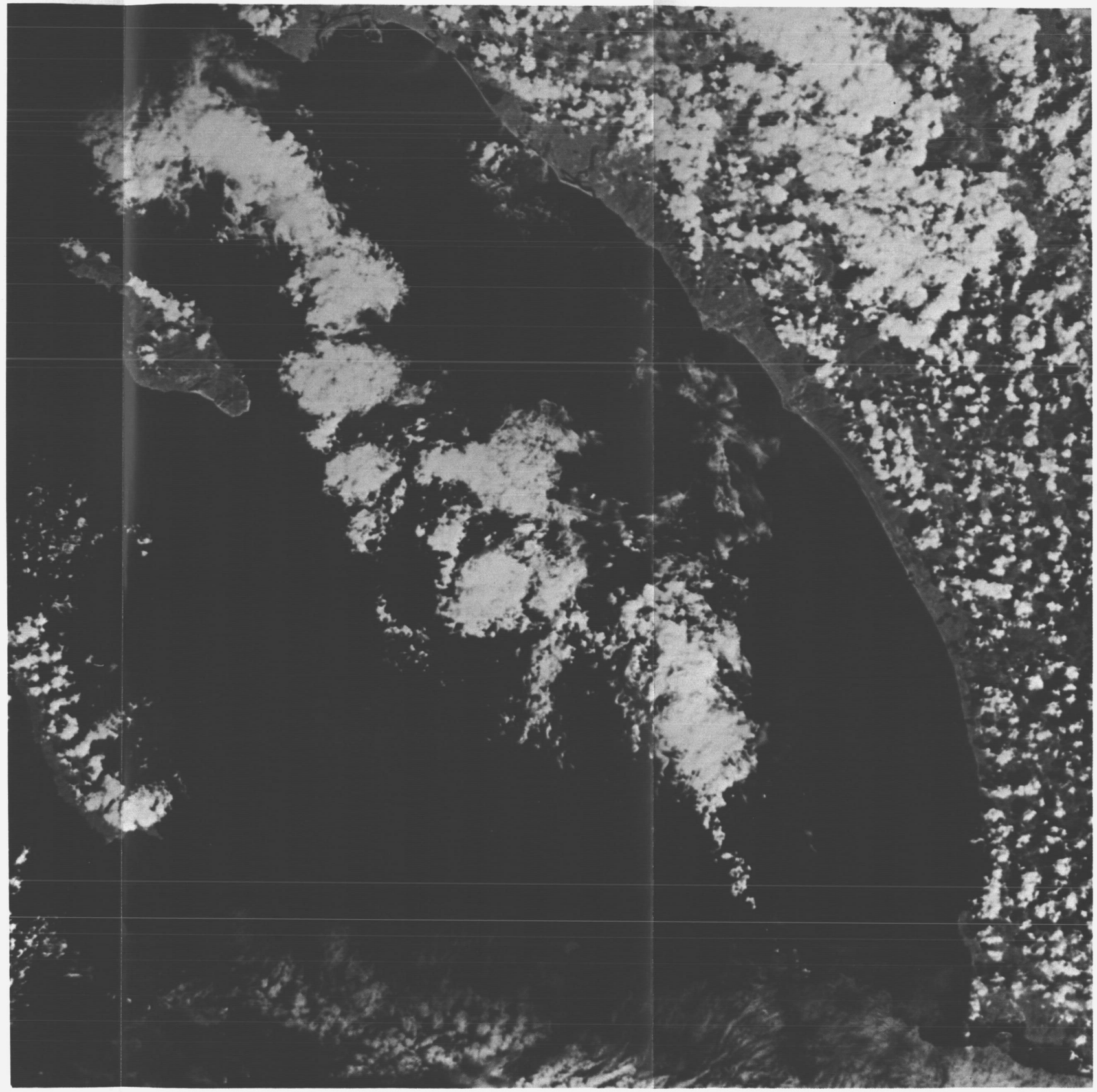

20% Cloud Coverage *Scale 1:603,400*

FIG. 8. APOLLO 9 PHOTOGRAPH AS 9-26A-3732A

AS 9-26-3747

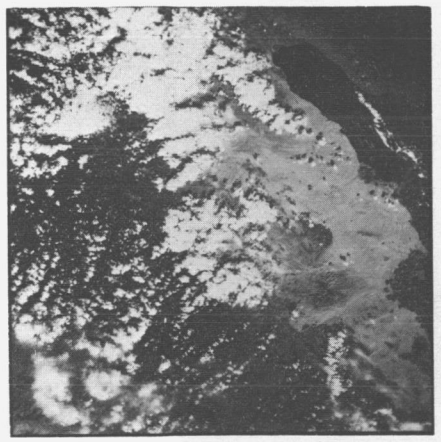

35% Cloud Coverage

AS 9-26-3748

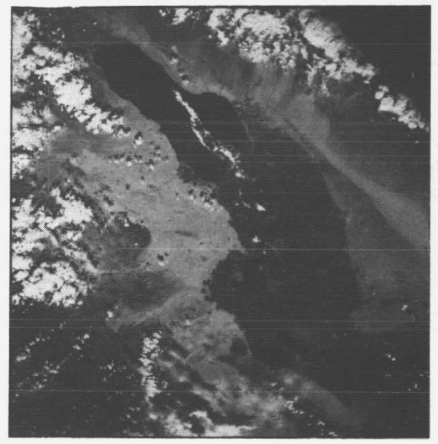

30% Cloud Coverage

Scale 1:2,386,000

FIG. 9. STEREOGRAM 3747/3748

Comments for Stereogram 3747/3748

Meteorology: Cloud forms visible in the stereogram are Cumulus Congestus, Cumulus Humilis, and Cirrocumulus.

Geography: Salton Sea and north-west reaches of the Imperial Valley can be seen in upper right of stereogram. Superstition Mountain and Vallecito Mountains appear in stereogram's center. San Felipe River flowing into south-west part of Salton Sea from Borrego Sink is not hidden by clouds. Interstate 8, just north of the Mexican border is seen leading into El Centro, California, in the southern half of the Imperial Valley. Crops under cultivation in Imperial Valley provide a sharp contrast to the desert area to the west.

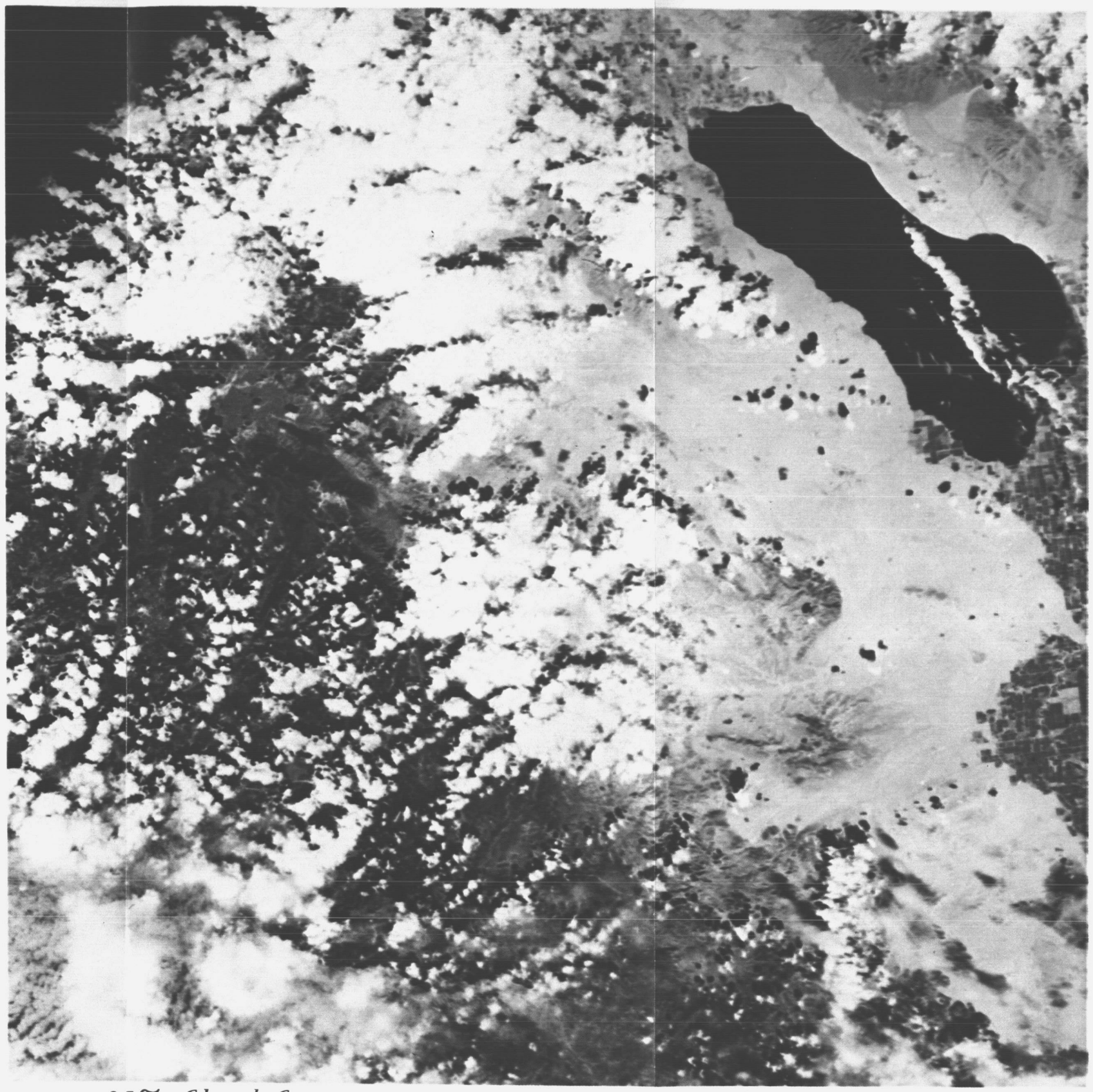

35% Cloud Coverage *Scale 1:586,400*

FIG. 10. APOLLO 9 PHOTOGRAPH AS 9-26A-3747A

AS 9-26-3707

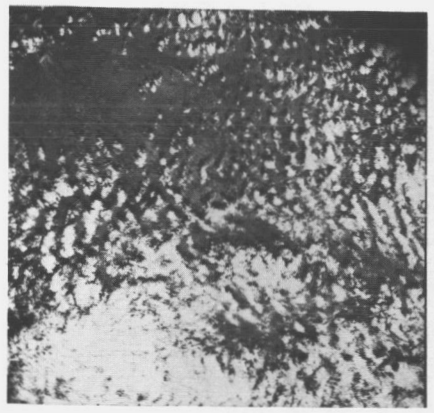

45% Cloud Coverage

AS 9-26-3708

55% Cloud Coverage

Scale 1:2,432,000

FIG. 11. STEREOGRAM 3707/3708

Comments for Stereogram 3707/3708

Meteorology: Cloud forms visible in the stereogram are Cumulus Humilis and Cumulus Congestus. When stuying this stereogram, whose component vertical photographs exhibit 45 percent (left) and 55 percent (right) cloud coverage, the observer can begin to get an appreciation of the effect of approximately 50 percent cloud coverage on the value of imagery taken from orbital altitudes on the order of 195 kilometers.

Geography: The principal point of the left hand photograph is located about 36 miles (57.9 km) north-west of Tucson, Arizona, just a few miles east of Interstate 10. The center of photograph 3708 is slightly south and to the east of that point. The Casa Grande National Monument Area and the Picacho Mountains are partially revealed in the upper left quadrant of the larger scaled 3707 photograph, shown adjacent to the stereogram.

After studying the first two stereograms showing cloud coverages of approximately 20 percent and 30 percent, it is quite apparent that vertical photography with approximately 50 percent cloud coverage makes conventional photo-interpretation processes very difficult. That is, normally visible landmarks, topographical features, and photo control points become very difficult to locate because of cloud interference.

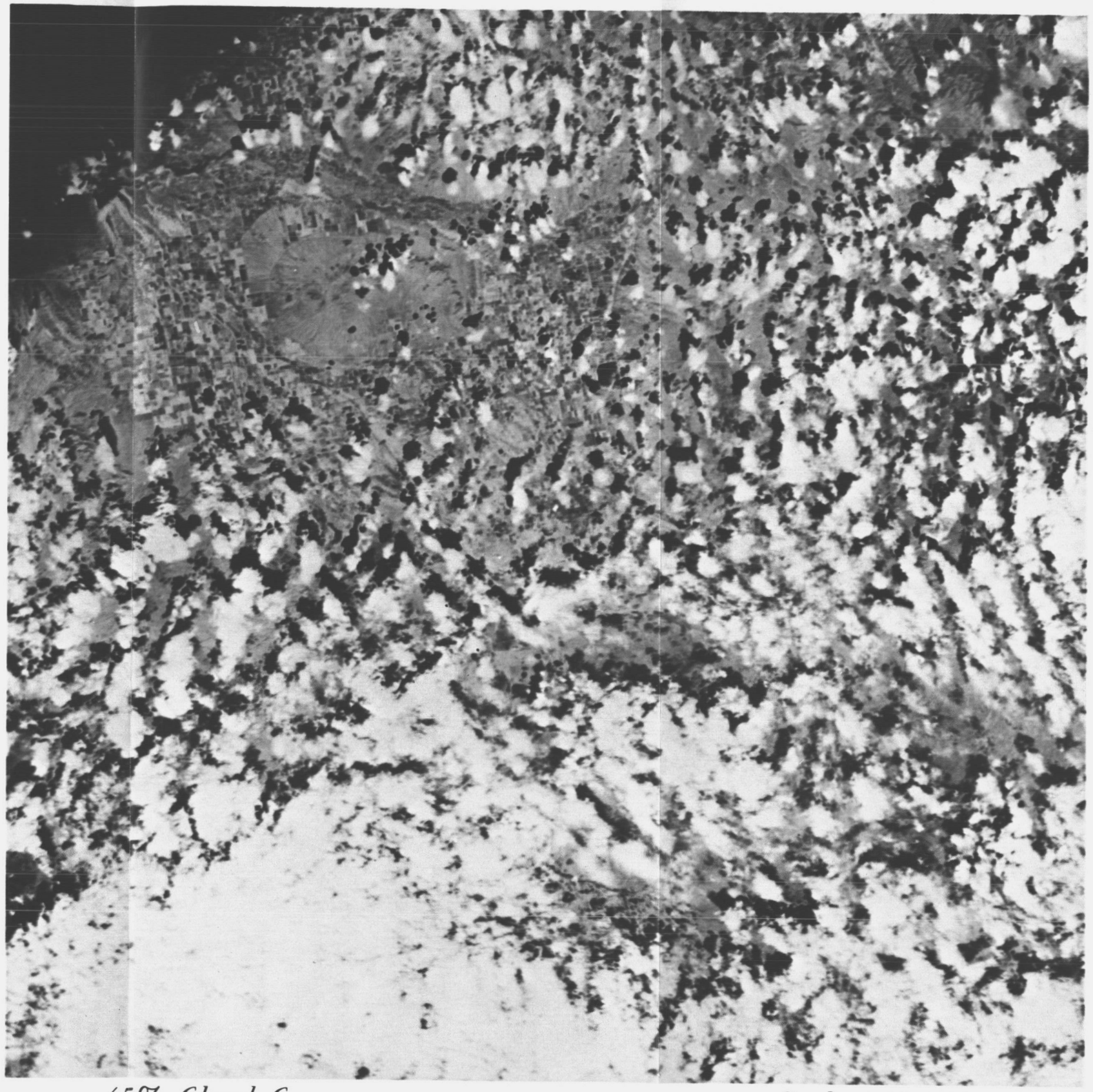

45% Cloud Coverage

Scale 1:597,800

FIG. 12. APOLLO 9 PHOTOGRAPH AS 9-26A-3707A

AS 9-26-3764

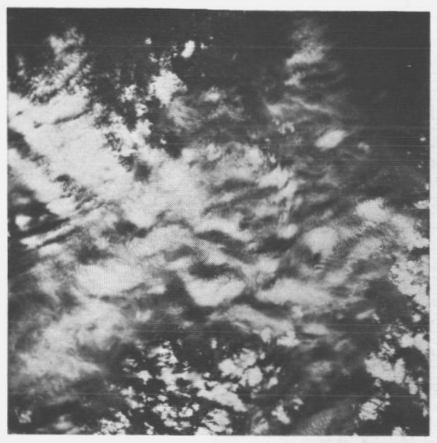

70% Cloud Coverage

AS 9-26-3765

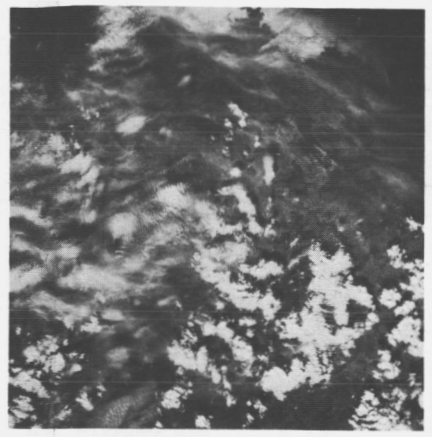

60% Cloud Coverage

Scale 1:2,409,000

FIG. 13. STEREOGRAM 3764/3765

Comments for Stereogram 3764/3765

Meteorology: Three distinct layers of cloud formations present themselves in this stereogram. The lowest (altitude) cloud formations are Cumulus Congestus and Cumulus Humilis. The next highest layer is Cirrocumulus, and the third or highest layer appears to be Cirrus and Cirrocumulus. The three distinct cloud layers can be differentiated readily when the photographs are viewed stereoscopically. To do this monoscopically (one photograph only) is practically impossible. This can be illustrated by viewing the above photographs stereoscopically for a few seconds until the three cloud levels are clearly envisioned, and then viewing monoscopically the larger scale photograph to the right.

Geography: These photographs provide coverage of parts of Querétaro and Hidalgo Provinces, north-west of Mexico City. Some of the complex volcanic, mountainous terrain can be seen on the eastern portion of the larger scale photograph 3765A. Some land under cultivation can be seen through the clouds, but very few terrain features can be positively identified, with this amount of cloud coverage.

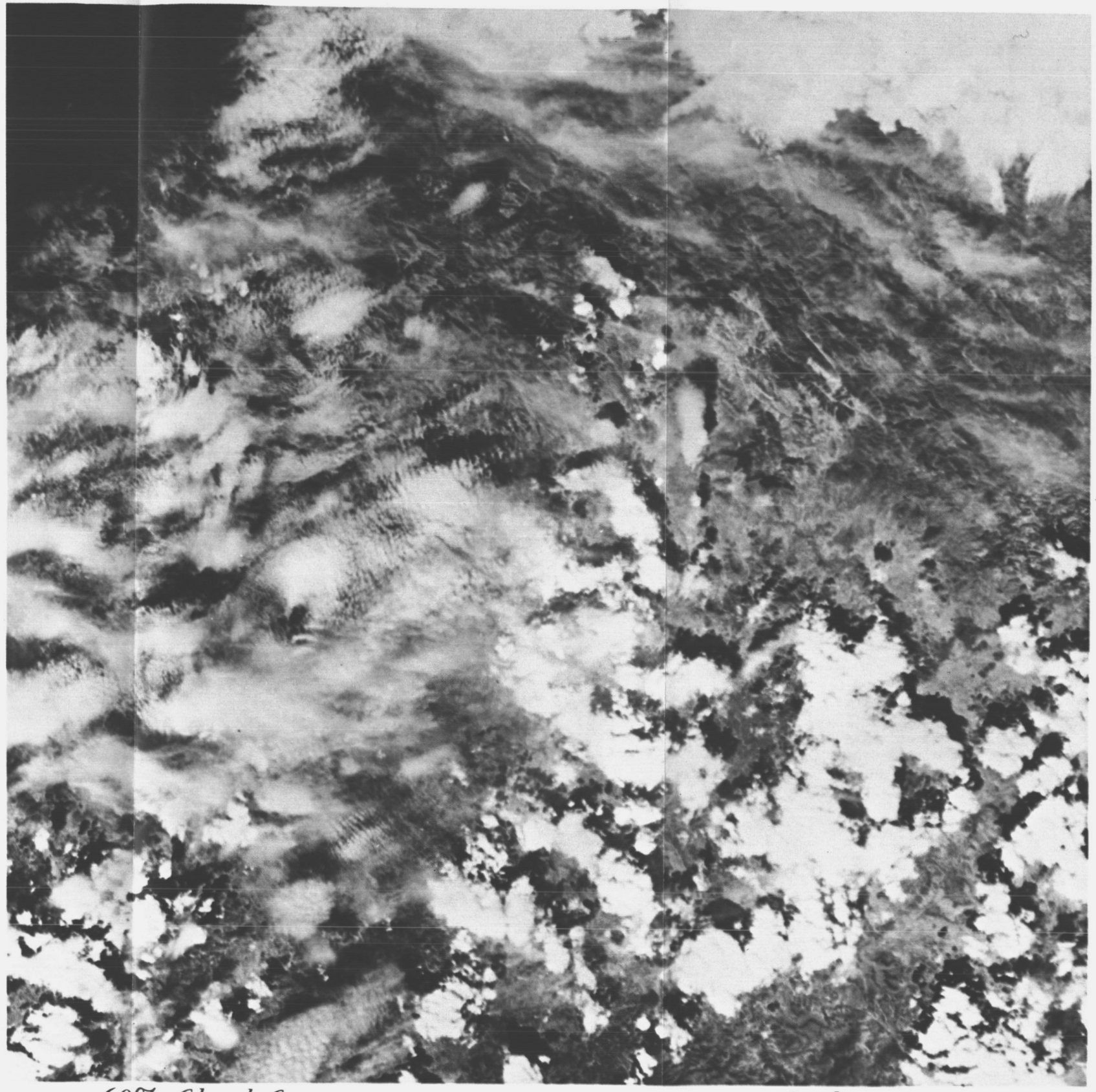

60% Cloud Coverage *Scale 1:592,000*

FIG. 14. APOLLO 9 PHOTOGRAPH AS 9-26A-3765A

V. A PATTERN RECOGNITION TECHNIQUE FOR DETERMINING CLOUD MOTIONS FROM SEQUENCES OF SATELLITE PHOTOGRAPHS

A Navy study contract N62306-69-C-0312 with the above title was completed by Stanford Research Institute (SRI) in April 1970, for Project FAMOS, Navy Weather Research Facility, Naval Air Systems Command, 3737 Branch Ave; Hillcrest Heights, Maryland, 20031. This summary, which describes several of the important elements of the SRI-Navy study, is included herein because of its potential interest to other researchers in the field of cloud cover analysis. The summary utilizes concepts, statements, and diagrams extracted from the final report of the study, dated April 1970 [3], and is not to be considered results of work by this author.

The study results describe an approach to the problem of extracting real time information, describing the direction and speed of cloud motions, from sequences of photographs of clouds. The cloud photographs which cover broad regions of the earth, were obtained by geosynchronous satellites ATS I and ATS III.

Cloud cluster centers, determined on the basis of area and brightness, are located using digitized representations of the cloud patterns in a photograph. The cluster centers are determined by a computer technique called "ISODATA" (Iterative Self Organizing Data Analysis) developed by SRI for pattern recognition. Cloud motion, indicated by the displacement of these centers in successive photographs, is handled by a separate computer program that matches centers found on two pictures. SRI researchers believe these techniques can be extended to include infrared data (closely related to cloud height) to be obtained by the next generation of synchronous satellites, thereby resolving certain height ambiguities existing in present cloud-motion computations. They also feel that computer techniques used in this study can lead to real-time, large scale computations of cloud motions over most of the globe, thereby providing information on winds and the dynamics of meteorological systems of various scales.

Dr. A. E. Brain of SRI suggested using a small number of cluster centers to represent a field of clouds. These centers, analogous to centers of gravity in mechanics, could be found on successive ATS photographs, and could be used to track the motions of cloud clusters. The ISODATA computer method, previously developed by SRI was suggested for this application.

A portion of an ATS photograph is digitized using a 120 × 120 array of points, giving a set of data in position and brightness (x, y, B). The data are then fed to the ISODATA program, which finds a set of cluster centers that describes the data. Then the same geographical area of a second ATS picture, for a later time, is digitized. ISODATA is then applied to the second picture, and the resulting differences between coordinates of the cluster centers in the two pictures are a measure of the displacement of the centers. These displacements are transformed into earth distances, and are divided by the time interval between photographs to give motion vectors of the cluster centers representing the clouds.

In summary, then, the sequence of steps for measuring cloud motions is as follows:

1. Landmarks are used for geographic registration of a series of ATS pictures.

2. Selected geographic regions are digitized (approximately 300 × 300 miles) using 120 × 120 locations and a 16-level gray scale. The same region is digitized at two different times to permit cloud motion tracking.

3. Cloud patterns in region at time 1 are represented by 10-20 cluster centers computed by ISODATA. Next, a corresponding set of cluster centers in same region at time 2 is computed.

4. Since displacement of cluster centers represents cloud movements in time interval from time 1 to time 2, the cluster centers must be paired, choosing one member from picture 1 and the second from picture 2. "MOTION PROGRAM" performs pairing, identifies typical displacement over the region, and then computes exact displacement between pairs.

5. Grid point analysis is made from cloud-motion vectors.

The logical procedures used in ISODATA are not described in this summary. They can be found, however, in Reference 3.

After ISODATA has determined the cluster centers in two photographs separated in time by an appropriate amount, the next objective is to formulate an automatic method for matching the cluster centers. If corresponding pairs of cluster centers are matched, and their locations at two times are known, then the displacement of a cluster center is its change in coordinates. The displacement along two axes divided by the time interval between pictures

gives the components of cloud motion. A practical difficulty encountered in matching centers is that a cloud group (and its center) may appear on one picture of a pair, but not on the other, because of dissipation or formation of a cloud group or movement of a group across a boundary of the digitized area. Accordingly, there may not be mates for all the cluster centers. The technique described in the following paragraphs copes with this problem, in that it matches those pairs that are "good" mates, and discards those centers not having a mate.

To illustrate this technique, assume that ISODATA has identified several cluster centers having coordinates (x_1, y_1) at time 1, and coordinates (x_2, y_2) at time 2. The hypothetical cluster centers at time 1 are shown in Figure 15 as "x"s, and the hypothetical centers at time 2 are shown in Figure 16 as "O"s. Figure 17 shows Figure 16 superimposed upon Figure 15. The centers shown on Figures 15 and 16 are numbered arbitrarily. From Figure 17, one can observe that center 3 at time 1 may be matched to center (1) at time 2; likewise, other pairs are 1 and (4), 2 and (2), 4 and (3), and 5 and (5). Centers 6 and (6) do not have mates. Figure 17 shows that the common displacement is one unit to the right and one unit down.

To determine the movement (displacement) automatically, a table is made showing the x differences between a center at time 1, and all centers at time 2; also, a table is made showing the y differences between a center at time 1, and all centers at time 2. These steps are shown in Tables 3 and 4.

By preparing a frequency distribution of the Δx entries in Table 3, it can be seen that the mode (most frequent value) is 1, as shown in Table 5. This is the desired x displacement. Similarly, by preparing a frequency distribution of the Δy entries in Table 4, it can be seen that the mode is -1, which is the y displacement, as shown in Table 6.

The next step in matching the pairs is to compute a table of Δx minus the mode (x_m) and a table of Δy minus the mode (y_m). These are shown as Tables 7 and 8. After the x and y displacements minus their respective modes are calculated (Tables 7 and 8), the "Fitting Function" is computed. The fitting function measures the deviation from the mode and is defined as

$$F = \sqrt{(\Delta x - x_m)^2 + (\Delta y - y_m)^2}$$

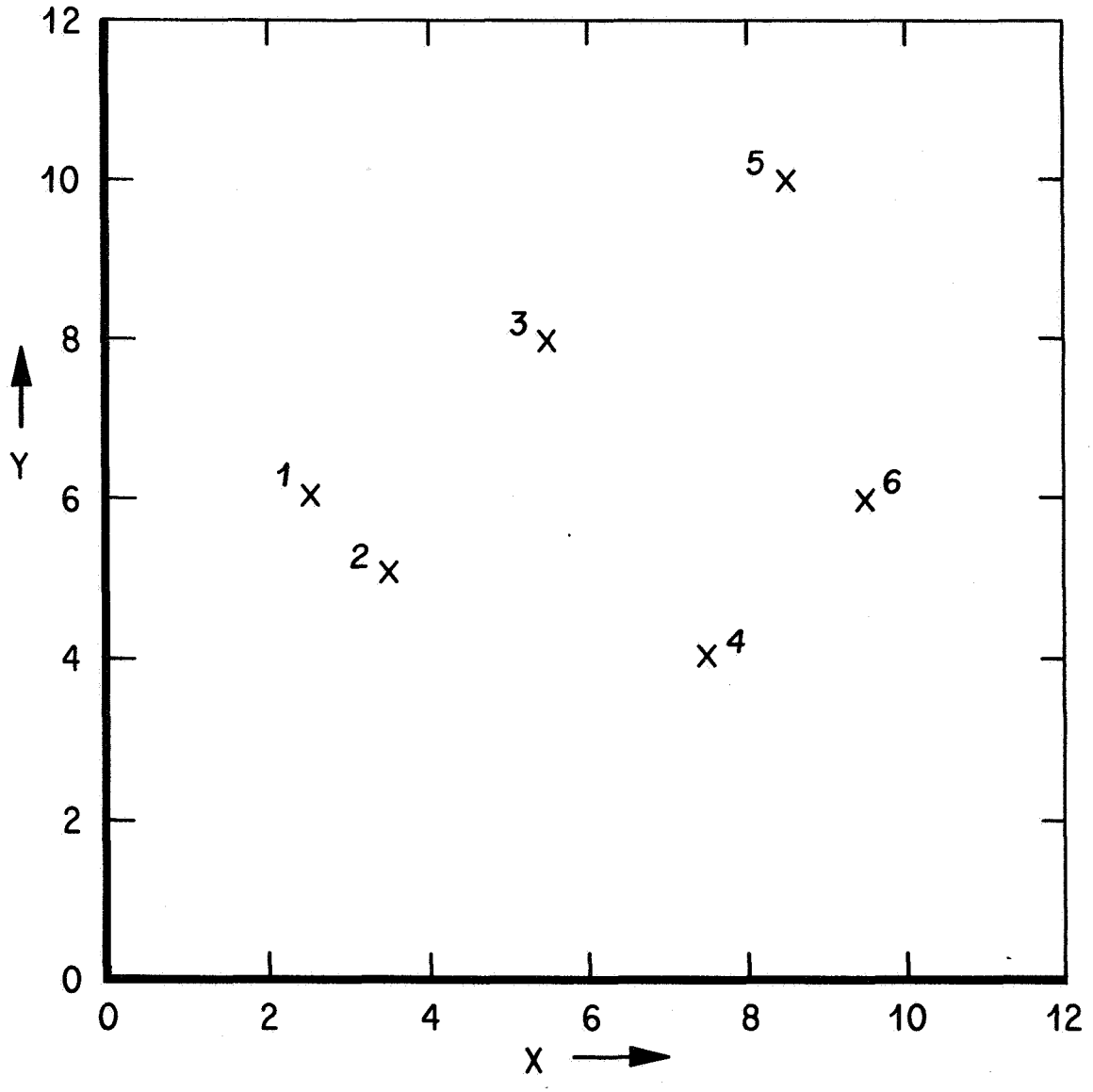

FIG. 15. HYPOTHETICAL CLUSTER CENTERS AT TIME 1

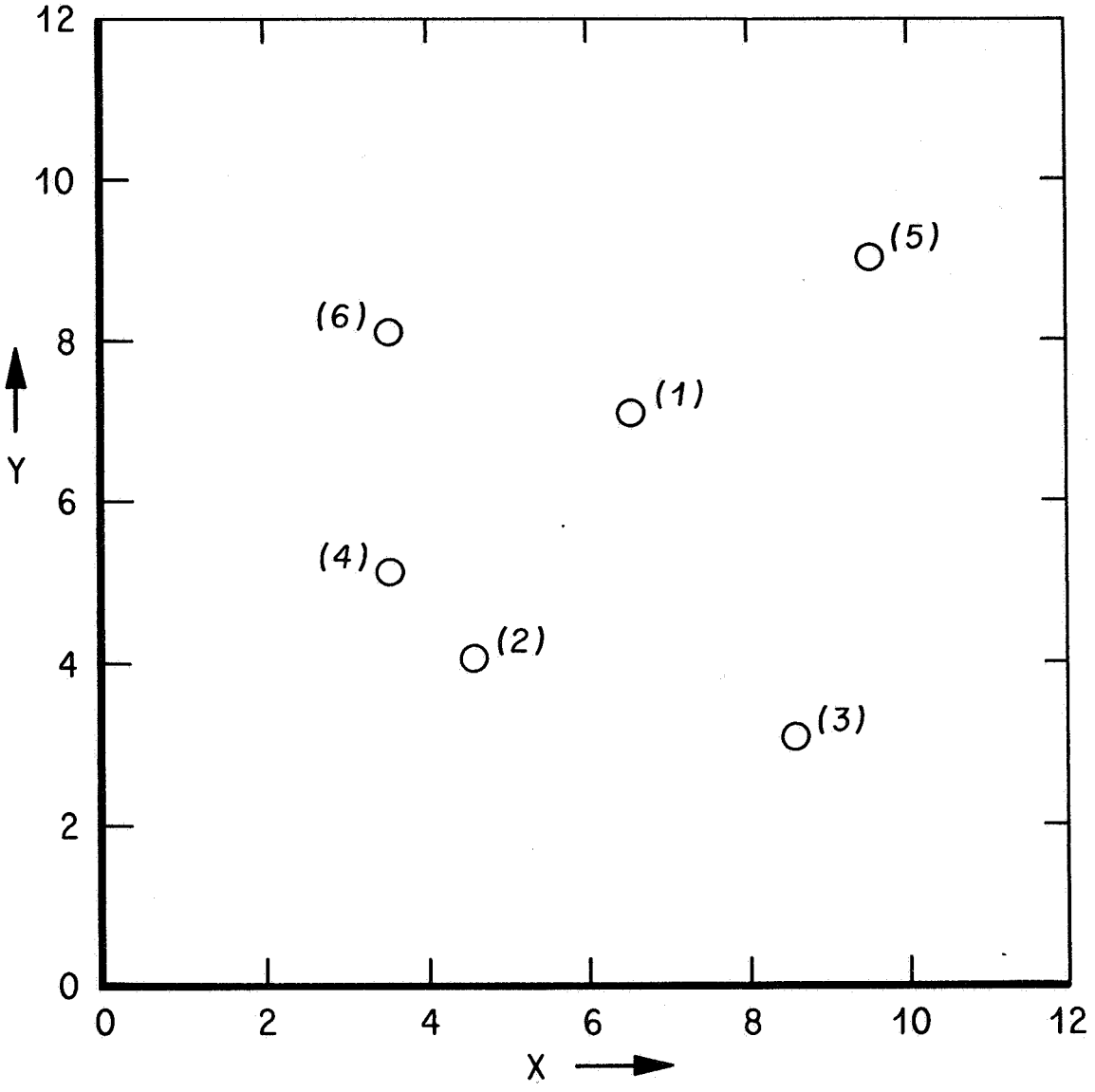

FIG. 16. HYPOTHETICAL CLUSTER CENTERS AT TIME 2

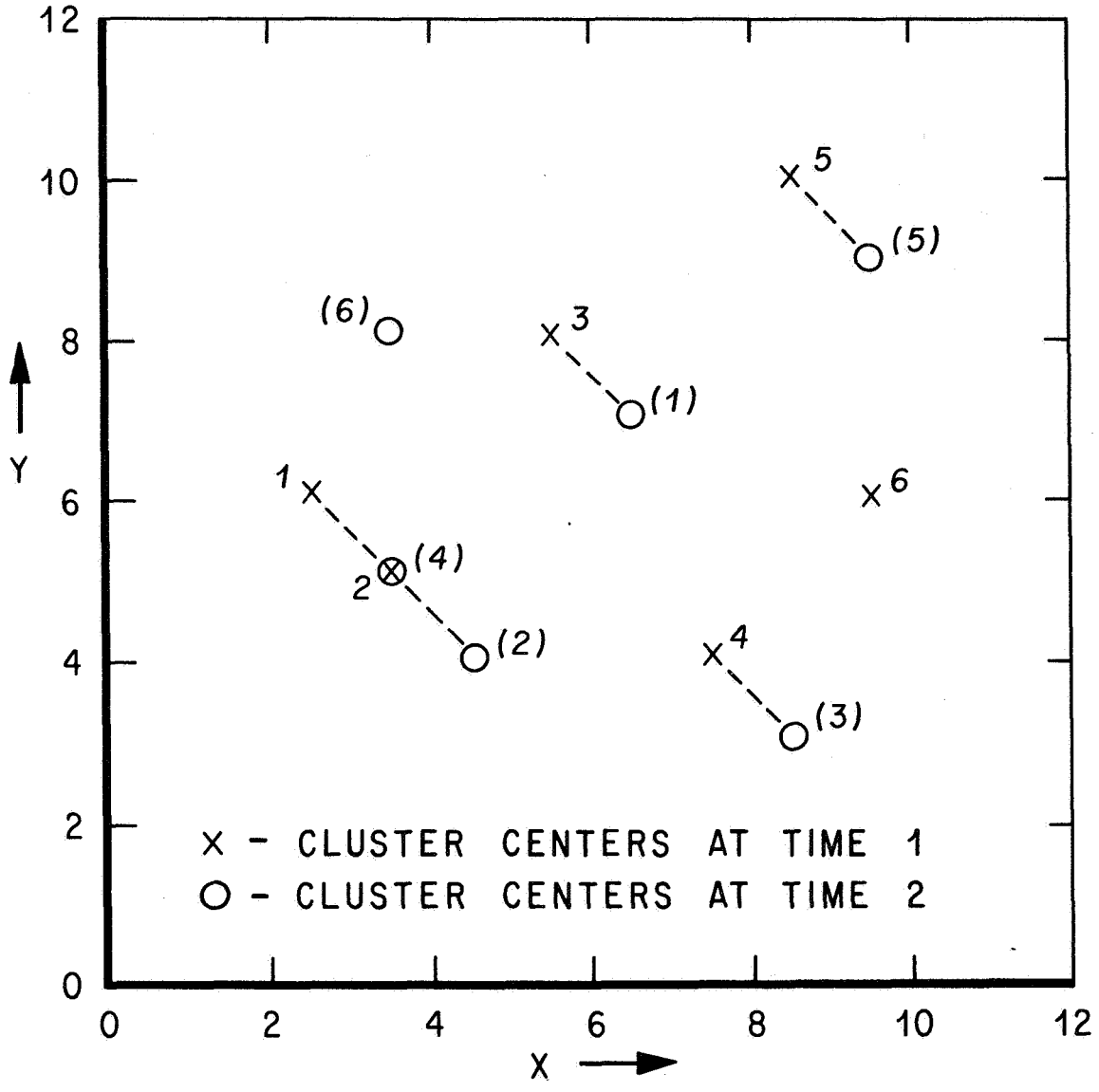

FIG. 17. FIGURE 16 SUPERIMPOSED UPON FIGURE 15

TABLE 3. Δx IN COORDINATES BETWEEN LOCATION OF A CLUSTER CENTER ON FIGURE 15 AND THE LOCATION OF CENTERS ON FIGURE 16, i.e., $\Delta x = x_{16} - x_{15}$

Cluster Centers on Figure 15	Cluster Centers on Figure 16					
	(1)	(2)	(3)	(4)	(5)	(6)
1	4	2	6	1	7	1
2	3	1	5	0	6	0
3	1	-1	3	-2	4	-2
4	-1	-3	1	-4	2	-4
5	-2	-4	0	-5	1	-5
6	-3	-5	-1	-6	0	-6

Example:

$$\Delta x_{(4)-4} = x_{(4)} - x_4 = 3.5 - 7.5 = -4$$

TABLE 4. Δy IN COORDINATES BETWEEN LOCATION OF A CLUSTER CENTER ON FIGURE 15 AND THE LOCATION OF CENTERS ON FIGURE 16, i.e., $\Delta y = y_{16} - y_{15}$

Cluster Centers on Figure 15	Cluster Centers on Figure 16					
	(1)	(2)	(3)	(4)	(5)	(6)
1	1	-2	-3	-1	3	2
2	2	-1	-2	0	4	3
3	-1	-4	-5	-3	1	0
4	3	0	-1	1	5	4
5	-3	-6	-7	-5	-1	-2
6	1	-2	-3	-1	3	2

Example:

$$\Delta y_{(6)-3} = y_{(6)} - y_3 = 8 - 8 = 0$$

TABLE 5. FREQUENCY DISTRIBUTION OF THE 36 VALUES OF Δx SHOWN IN TABLE 3

Value	Frequency of Occurrence in Table 3
-6	√√
-5	√√
-4	√√√
-3	√√
-2	√√√
-1	√√√
0	√√√√
1	√√√√√√
2	√√
3	√√ Therefore, +1 is mode
4	√√ in x displacement
5	√√ (x_m)
6	√√
7	√

TABLE 6. FREQUENCY DISTRIBUTION OF THE 36 VALUES OF Δy SHOWN IN TABLE 4

Value	Frequency of Occurrence in Table 4
-7	√
-6	√
-5	√√
-4	√√
-3	√√√
-2	√√√√
-1	√√√√√√√
0	√√√
1	√√√
2	√√√ Therefore, -1 is mode
3	√√√√ in y displacement
4	√√ (y_m)
5	√

TABLE 7. x DIFFERENCES MINUS THE MODE ($\Delta x - x_m$) FOR Δx VALUES OF TABLE 3 ($x_m = +1$)

Cluster Centers on Figure 15	Cluster Centers on Figure 16					
	(1)	(2)	(3)	(4)	(5)	(6)
1	3	1	5	0	6	0
2	2	0	4	-1	5	-1
3	0	-2	2	-3	3	-3
4	-2	-4	0	-5	1	-5
5	-3	-5	-1	-6	0	-6
6	-4	-6	-2	-7	-1	-7

Example:

$$\Delta x_{3,(5)} - x_m = 4 - 1 = 3$$

TABLE 8. y DIFFERENCES MINUS THE MODE ($\Delta y - y_m$) FOR Δy VALUES OF TABLE 4 ($y_m = -1$)

Cluster Centers on Figure 15	Cluster Centers on Figure 16					
	(1)	(2)	(3)	(4)	(5)	(6)
1	2	-1	-2	0	4	3
2	3	0	-1	1	5	4
3	0	-3	-4	-2	2	1
4	4	1	0	2	6	5
5	-2	-5	-6	-4	0	-1
6	2	-1	-2	0	4	3

Example:

$$\Delta y_{5,(3)} - y_m = -7 - (-1) = -6$$

Fitting function values are shown in Table 9. The cluster pairs shown earlier in Figure 17 are identified in Table 9 by zero entries.

The modal displacement values x_m and y_m define a vector that is the most common translational component; entries in Table 9 are the length of the deviation of each displacement from the modal value. In real cases involving cloud pictures, there are no entries that are exactly zero. However, relatively small values appearing in the fitting function table denote pairs. Steps in processing the fitting function table are as follows: The smallest entry is found; this entry denotes the first pair. The vector joining these two centers is the best match to the vector defined by the modal values. These two centers are then removed from further consideration by deleting the remaining entries in the same row and column of the table. This pair matching process is continued until the remaining entries in the fitting function table are all larger than a specified threshold value, at which time the remaining points are discarded.

TABLE 9. FITTING FUNCTION, $F = \sqrt{(\Delta x - x_m)^2 + (\Delta y - y_m)^2}$

Cluster Centers on Figure 15	Cluster Centers on Figure 16					
	(1)	(2)	(3)	(4)	(5)	(6)
1	3.6	1.4	5.4	0	7.2	3
2	3.6	0	4.1	1.4	7.1	4.1
3	0	3.6	4.5	3.6	3.6	3.2
4	4.5	4.1	0	5.4	6.1	7.1
5	3.6	7.1	6.1	7.2	0	6.1
6	4.5	6.1	2.8	7	4.1	7.6

Example:

$$F_{(3),3} = \sqrt{\left[\Delta x_{(3),3} - x_m\right]^2 + \left[\Delta y_{(3),3} - y_m\right]^2}$$

$$= \sqrt{(3 - 1)^2 + [-5 - (-1)]^2}$$

Therefore,

$$F_{(3),3} = 4.5$$

SRI researchers found that the fitting function could be improved further by including brightness "B", as well as location x, y, because a matched pair of cluster centers should have about the same average brightness on both pictures. Brightness can be included in the fitting function F by introducing $(\Delta B)^2$ under the radical.

SRI has developed a method of matching landmarks in a series of pictures, thereby obtaining accurate geographic registration. This process uses a TV display device which gives the human operator controlled access to sequences of pictures and a zoom capability. The position data are fed directly to a computer. This scheme eliminates discernible effects of satellite motions and other sources of uncertainty in registration. This improved scheme was not available at the start of the study; accordingly a less accurate method, described later on in this summary, was used.

A schematic diagram and photograph of the components of equipment which were used in this study are shown in Figure 18 (extracted from Reference 3.) The cloud photograph is precisely positioned on the light box using the verniers of a microscope stage, thereby controlling the geographic location of the area scanned by the lens and TV camera. The lens views an area approximately 300 × 300 miles (483 × 483 km) which can be magnified and viewed on the TV monitor. The TV camera leads to an analog-to-digital converter which is connected to the SDS 940 computer. Digitizing is done for 120 × 120 locations to cover the area viewed using a 16 level gray scale. The computer is controlled from a teletype terminal and the digitized data are stored on magnetic tape. After viewing one location, the verniers are moved to view the next location, to allow a controlled strip of overlap with the previous region of about 30 percent. This permits the border of one region to fall well inside its neighboring region, so that motions found near the borders may be discarded in favor of the more representative coverage of the same data in the interiors of the neighboring regions.

According to SRI researchers, the 120 × 120 array mentioned earlier proved to be rather cumbersome for the computer, therefore the array size was reduced to 30 × 30 by selecting every fourth point along the X and Y axes. The resultant arrays retained the photograph's pattern structure and sped up computations of cluster centers. Figure 19-B is a 30 × 30 array, which is a digitized representation of Figure 19-A, which in turn is part of a cloud photograph obtained by the ATS-1 Geosynchronous Satellite on May 25, 1968, over the central part of the Pacific Ocean. Figure 20 shows the cloud pattern of Figure 19-A, represented by dots, and 12 cluster centers, represented by "C"s determined by ISODATA. The next step in determining cloud motions

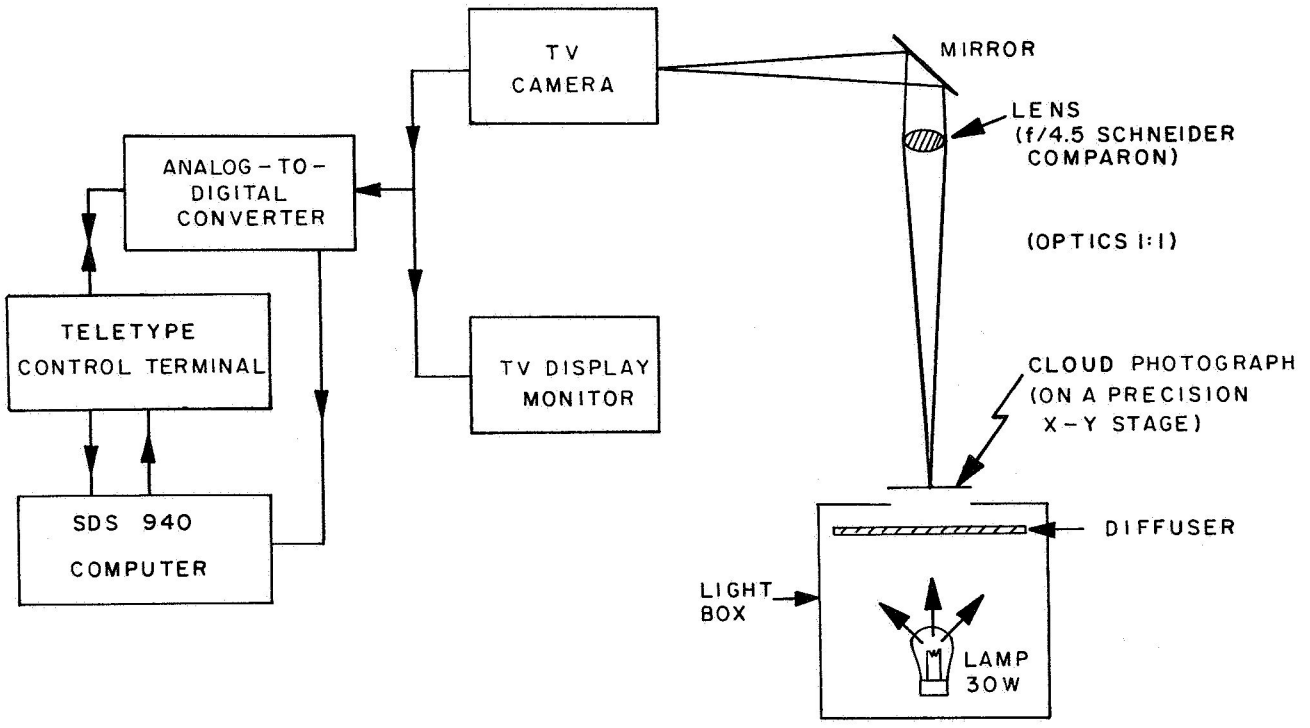

a) Schematic Diagram of the Equipment Used In Digitizing Portions of Application Technology Satellite (ATS) Pictures.

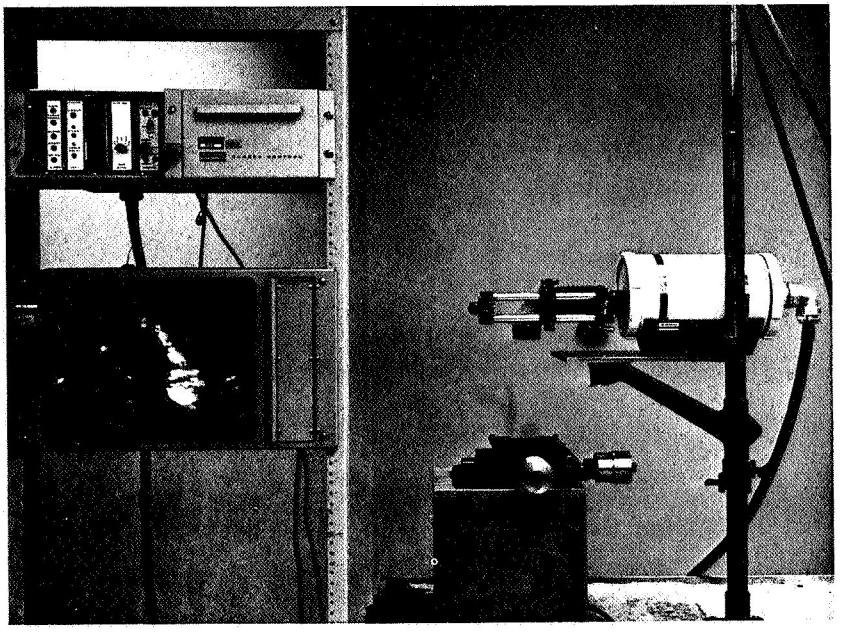

b) A View of the Digitizing Equipment. The Cloud Pattern Being Digitized Is Shown On the TV Monitor.

FIG. 18.

a) Part of a Cloud Photograph Obtained By the ATS-1 Geosynchronous Satellite On May 25, 1968. The Photograph Was Made from the TV Display Monitor Used In the Digitizing Process.

```
    1  5  9 13 17 21 25 29 33 37 41 45 49 53 57 61 65 69 73 77 81 85 89 93 97101105109113117
117    7 10  9  7  6                                                                    117
113       8  9  7                                                    8                  113
109       6 10  7  7                                          6  6  7  6  6              109
105          8  6  6  6                                             8  6                 105
101             6  9  8  6                                                               101
 97             6  8 10  7  8  6                                    6                    97
 93             8 10 10  8  6                                             6              93
 89             6  9 10 10  7  6                                                         89
 85                   8  7  6  6  6  6                                                   85
 81                      6  6  6                                    6                    81
 77                   6  7  6  6  6  6                              6  7  6  6           77
 73                8  9  9  9  8  6  7  8                           7  8           6     6  73
 69             6  7  9  6  6  7                                    7  8  8  7  6        69
 65             6     6                    6  6                    6  7  6  6  7        65
 61                      6     9  7  7  7  6                       6  6           6     61
 57             6        7  6  7  8  6  6  6  6                    6                    57
 53          6  7  7  9  7  7  7  7  6                                                   53
 49             8 10 10 10  9  9  9  6  6     6                                       49
 45                9 11 10 11 11  9  8  7                                             45
 41                6  9 11 11 10 10  7  6                                             41
 37                      6  7  6  6                                                   37
 33                         6  6  6                                                   33
 29                                                                                   29
 25                                                                                   25
 21                                                                                   21
 17                                                                                   17
 13                                                                                   13
  9                                                      8  6  6                      9
  5                                                   6     6     6                    5
  1                                                   7  7  6  6  9  7  7  7  6  6  6   1
    1  5  9 13 17 21 25 29 33 37 41 45 49 53 57 61 65 69 73 77 81 85 89 93 97101105109113117
```

b) A Digitized Representation of Figure 19a Using a 30-by-30 Matrix of Locations and a 16-Level Gray Scale (0,1,2,---15).

FIG. 19.

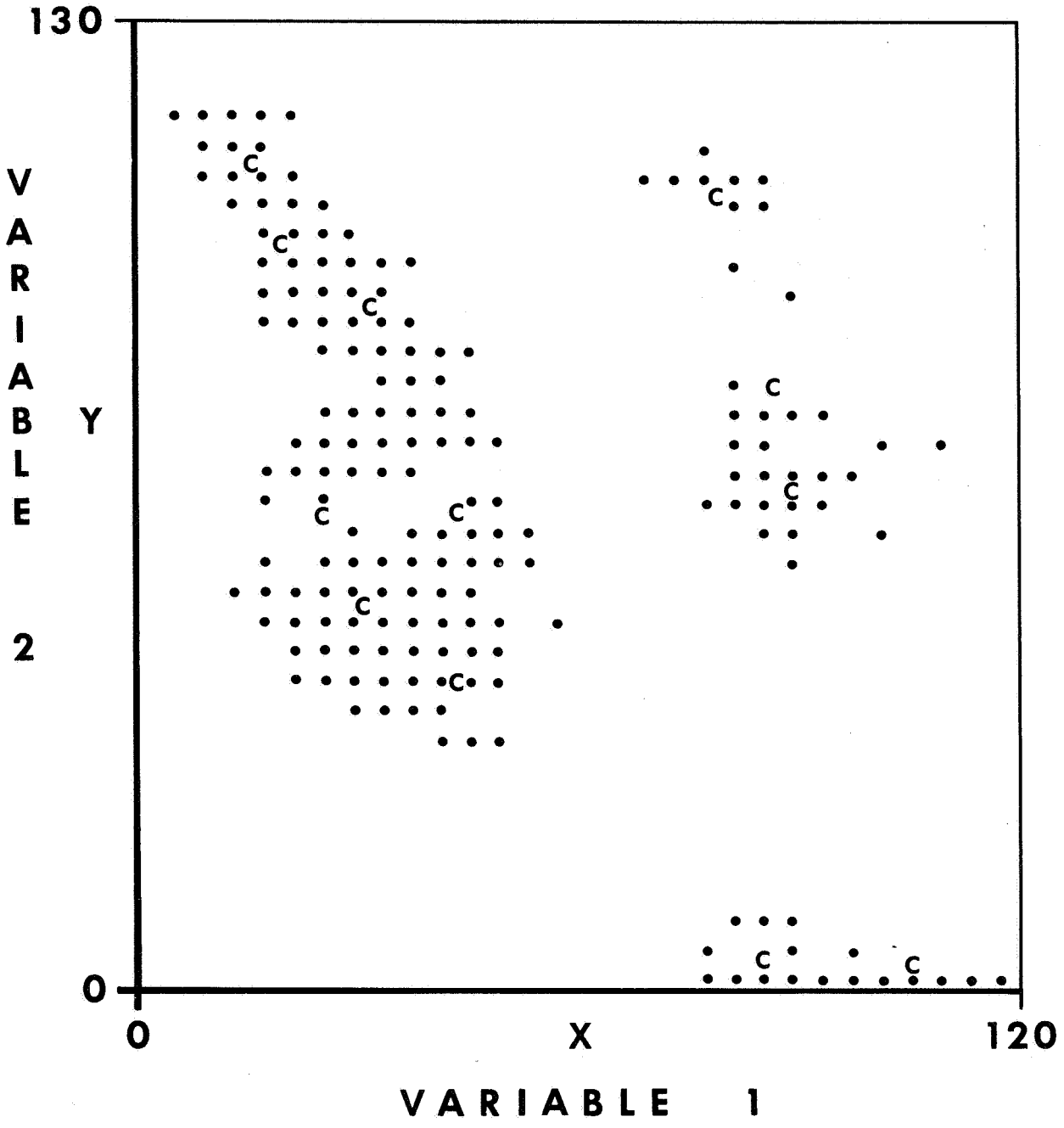

FIG. 20. A DISPLAY OF THE CLOUD PATTERN OF FIGURE 19a AS DOTS, AND CLUSTER CENTERS (C's) DETERMINED BY THE ISODATA PROGRAM

is to apply ISODATA to a picture of the same geographical region at a later time. SRI researchers found that one to two hours was a reasonable time interval.

A critical part of the analysis was found to be the application of ISODATA so that cluster centers found on the second picture of a geographical region could be matched with those at the earlier time, thereby giving displacements and motions of clusters. The best strategy found by SRI was to obtain a first estimate of the general cloud displacement, and to use this in repositioning the centers from picture 1 as the "initial guess" centers on picture 2. The initial guess centers, relocated by ISODATA on picture 2, tend to stay with the same cluster as on the first picture. To obtain a first estimate of the general cloud displacement within the region, one finds eight cluster centers on picture 1 by ISODATA. Eight centers are obtained independently in like manner on picture 2. The two sets of centers are fed to the matching program, and for those pairs selected, average displacements along X and Y axes are found. These tentative displacements are applied to the cluster centers of picture 1, using a "sphere factor" (determines radius of the cluster) to reposition them as initial guess centers for the final analysis of picture 2.

In Figure 21, the 1's denote locations of cloud elements at 2047 G.m.t. on 25 May 1968 (same data as Figure 20). Corresponding positions of cloud elements two hours later are indicated by 2's. This diagram indicates that the motion of the major cloud band on the left side of the region is toward the southwest. Other motions apparent upon inspection are similar except that the 1's in the lower right corner disappear. This is also consistent with a general southwestward motion in the region.

The above computer procedure gives the same result as human deduction. Cluster centers (C's) in Figure 20 were displaced using the average motion of eight centers in pictures "1 and 2" found by ISODATA. The displaced centers used as initial guesses on picture 2 were repositioned to give an optimum fit. Centers on picture 1 are shown by 1's in Figure 22, and the final centers on picture 2 are shown by 2's in Figure 22. The motion program selected the pairs connected by lines in the order a, b, c, d, e, f, g, h. These pairs agree quite well with one's intuition, except for line g and the broken line i. Since the motion program matches pairs using brightness as well as position coordinates, and since the average brightness of the cluster indicated by 1 in line g is 66 and by 2 in line g is 64, points 1 and 2 on line g were paired. Clusters 1 and 2 of line i had brightness values of 95 and 85, respectively. The motion program did not accept them as a pair, however, it was believed possible that they represented a high bright cloud that moved in a different direction from the main cloud mass.

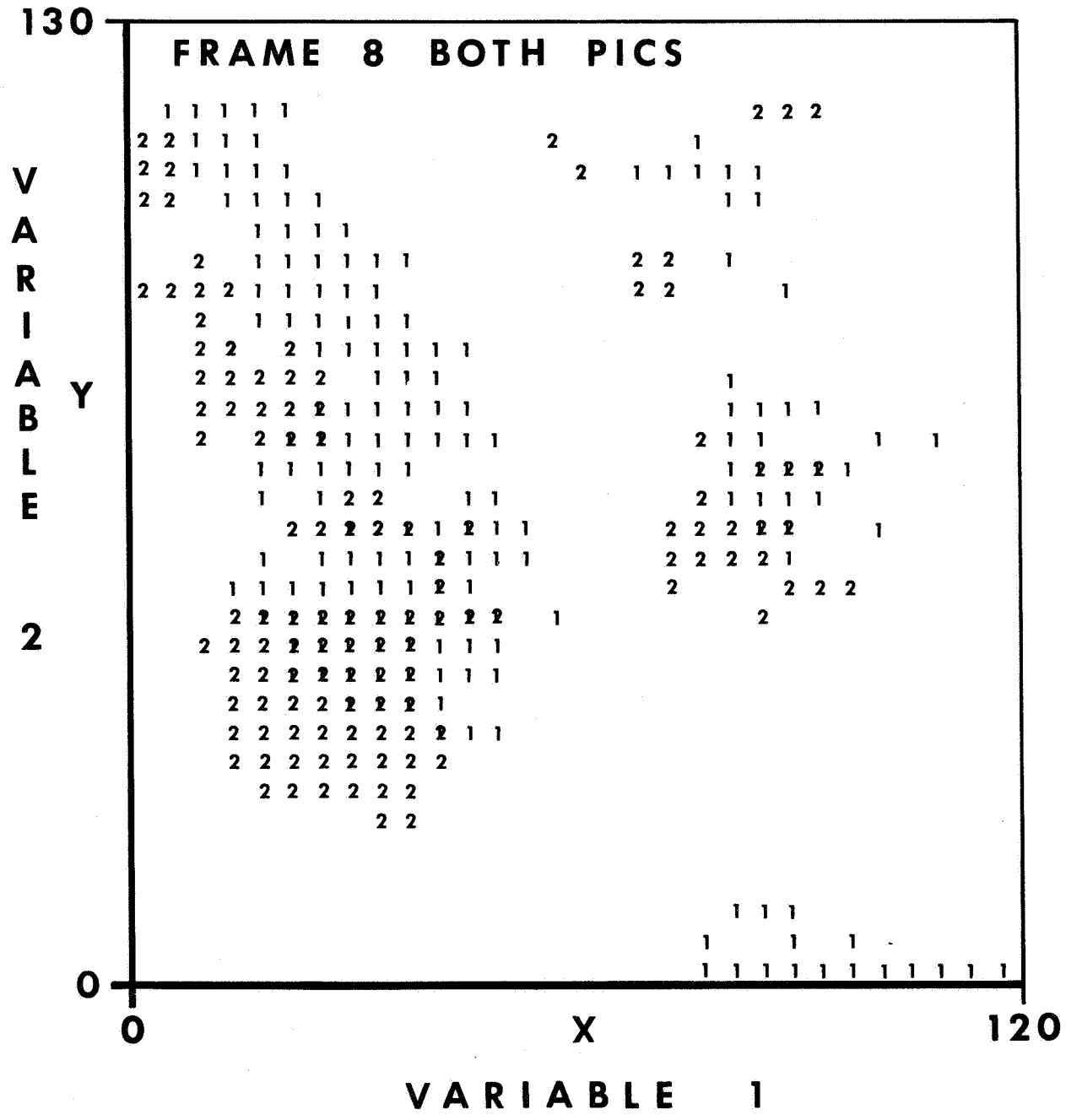

FIG. 21. A CATHODE RAY TUBE DISPLAY OF CLOUD PATTERNS AT 2047 GMT (TIME 1) AND 2246 GMT (TIME 2), 25 MAY 1968. *The 1's denote positions of cloud elements at time 1. (These are the same data as in Figures 19 and 20.) The 2's denote clouds at time 2. This presentation is made directly from the control console of the CDC 3300 computer. The pattern motion is obviously toward the southwest.*

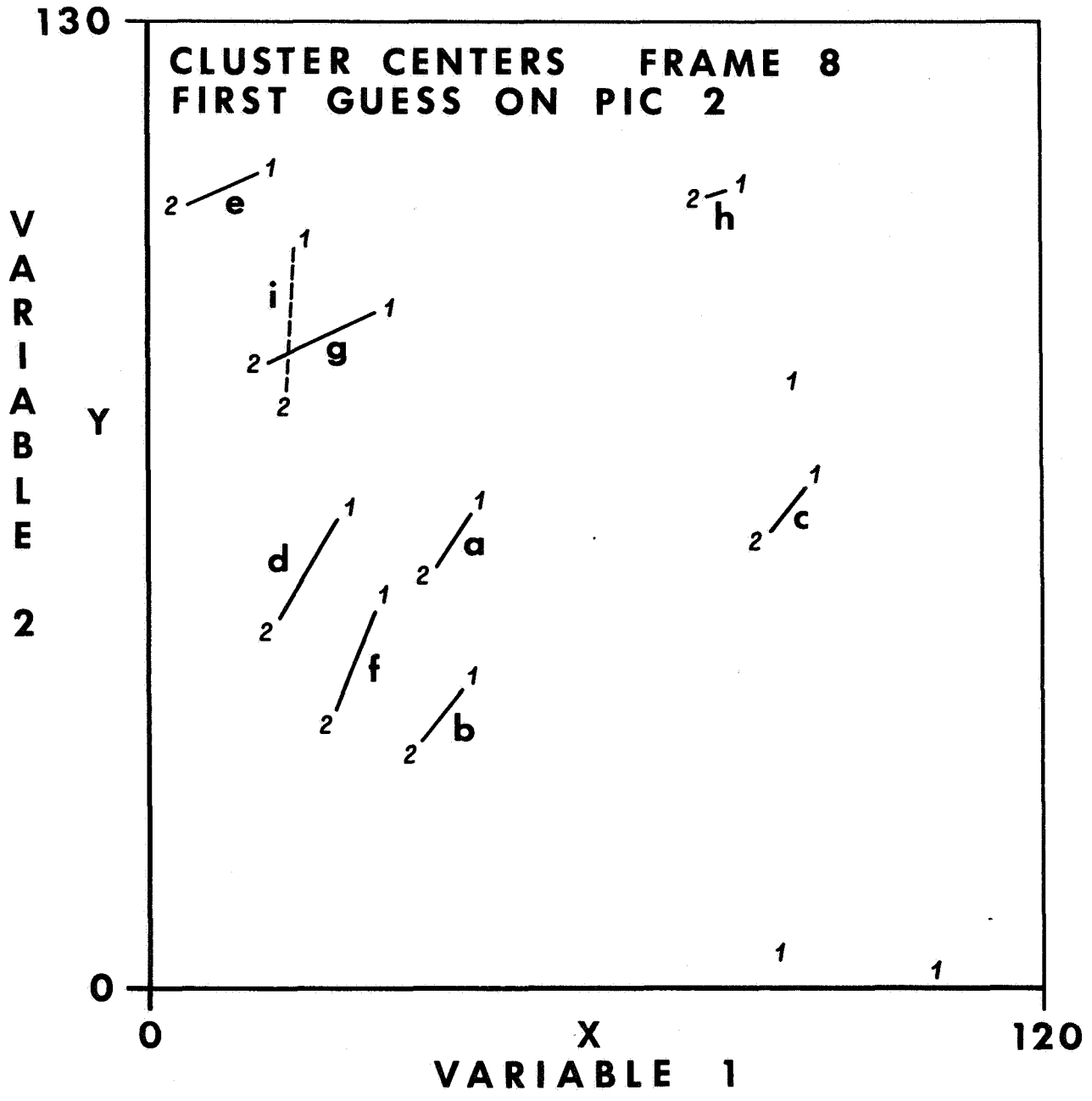

FIG. 22. CLUSTER CENTERS AT TIME 1 REPRESENTED BY 1's AND AT TIME 2 BY 2's. *Compare cluster centers to cloud patterns of Figure 21. Pairs were matched by the Motion program in the order a,b,c,--h. Cluster center displacements in two hours are from 1's to 2's.*

SRI researchers concluded that the three-dimensional fitting minimizes brightness changes and gives a better tracking of the same cluster than could be obtained using position information alone. They concluded further that the field of these motions has a degree of smoothness that is meteorologically acceptable. The same area shown in the preceding figures was also manually viewed on the TV console using ATS pictures for the entire day, and the qualitative sense of the motion agreed well with that obtained by the scheme discussed herein.

In summary, this study by SRI for Project FAMOS of the Navy Weather Research Facility, demonstrated that cloud motions depicted by recent observations of cloud positions and brightness from the ATS geosynchronous satellites can be processed by computer to quantitatively measure the motions. Infrared measurements from future satellites are expected to add greatly to the value of the data by providing cloud height information. SRI stated that their procedure can be modified easily to include this new variable. They believe that a completely automatic system appears feasible and that the goal of obtaining cloud motions over much of the globe in real time may be attainable within a few years.

Analytical studies pertaining to direction and velocity of cloud motions, have received less emphasis in the past than analyses relating to cloud cover and cloud type with respect to remote sensing mission implications. This Navy technique is especially pertinent to photogrammetric analyses of cloud phenomena, due to its strong dependence on sequential orbital photographic imagery. The cloud motion and height determination technique, as predicted feasible by SRI, may be quite worthy of consideration for use in future earth remote sensing missions. Perhaps the real time knowledge of cloud motion obtained by geosynchronous satellite could be coupled with in-flight mission planning efforts of orbiting remote sensing station crews. Conceivably, this could result in a greater yield of remotely sensed data in the several spectral bands which are affected by cloud cover to varying degrees. In short, the remote sensing station crews would be appraised of which geographical areas of interest will be free of clouds, and when they will be clear, due to the cloud intelligence provided by this technique. Sensing plans for ensuing orbits could thereby be more efficiently made.

VI. CLOUDS AND OTHER ENVIRONMENTAL FACTORS AFFECTING AERIAL PHOTOGRAPHIC MISSIONS

Season and weather must both be considered when planning an aerial photographic mission. For example, if the intended use of the photography is terrain contouring (topographic mapping), then a season for conducting the photographic mission should be chosen such that deciduous trees are bare.

Elements of our natural environment which affect aerial photography are clouds, turbulence, haze, and solar altitude. Turbulent air, in the case of aircraft flown photography, bounces the aircraft and causes image motion on the exposed film, thereby decreasing the quality of definition of photographic images. As altitude increases, this effect is worsened, since photographic scale decreases with altitude, with an attendant deterioration in image interpretability. Spacecraft-flown photography is, of course, not confronted by this particular aspect of the weather.

Haze in the atmosphere, caused by the scattering of blue and ultraviolet energy, has an overall degrading effect on aerial photography, particularly color photography. Haze decreases image definition, impairs the photographic qualities of tone and texture, and in color film, it causes the colors to appear somewhat faded or washed out, compared to the true colors which would be recorded on a relatively haze-free day. A 15 mile (24.1 km) visibility generally indicates an acceptable level of haze for aircraft photographic mission planning purposes.

A 30-degree sun angle is usually the minimum solar altitude at which aerial photography is flown so as not to record objectionably long shadows. The time-span in any particular day during which the solar altitude is greater than a minimum allowable value is known as "the photographic day length." The length of the photographic day and its beginning time and ending time can be determined readily by using solar altitude nomograms. Knowing the date of the planned photography, the minimum allowable solar altitude, and the latitude of the area to be photographed, one can readily determine the time during any day when the solar altitude requirement is met. One source of solar altitude nomograms is the "Manual of Color Aerial Photography," published by the American Society of Photogrammetry.

The last, but perhaps the most important, principal element of natural environment affecting aerial photographic mission planning, is cloud cover. The generally accepted practice is to conduct aerial photographic missions

when cloud cover is less than 10 percent, and the solar altitude, haze, and turbulence conditions are within acceptable limits. The National Oceanic and Atmospheric Administration has compiled statistics which can be used when one is trying to determine, in advance, months or seasons which are optimum for taking aerial photographs. The National Oceanic and Atmospheric Administration has published this information as a series of 12 monthly maps from which one can predict the number of days per month that will experience 10 percent or less cloud cover in any area of the United States. Such a map for the month of July is shown as Figure 23. As shown in this example, North Alabama can expect from three to six days in July which will be clear (10 percent or less cloud cover) from sunrise to sunset, and which will meet the 30 degree solar altitude criteria; northeast Florida, and Boston, Massachussets can also expect three to six days; western New York State, six to eight days; and Juneau, Alaska, one to three days. This illustrates then that, at least for aerial photographic mission planning purposes, this type of statistical information is quite helpful.

In some instances the presence of high cirrus clouds, which are delicate and fibrous, has a somewhat beneficial effect on photographic quality by reducing shadow intensity and softening the light. The desirability of this, however, depends on the intended purposes of the photography.

The Aerospace Environment Division of Aero-Astrodynamics Laboratory, Marshall Space Flight Center, has sponsored cloud cover model research concerned with "Simulating the Consequence of Cloud Cover on Earth-Viewing Space Missions"(4). In the referenced work, the consequence of cloud cover on Earth-photographing space missions was evaluated by a Monte-Carlo computer simulation procedure, using world-wide cloud cover statistics. These cloud data contain probability distributions for five cloud-cover categories arranged by reference periods. Spatial and temporal probability values are included to account for cloud persistence. This was one phase of MSFC's cloud cover model work. The overall goal of this research is to produce atmospheric attenuation models to predict degradation effects for all classes of sensors for application to earth-sensing experiments from spaceborne platforms. To insure maximum utility and application of these products, the developmental work has been coordinated with NASA Headquarters and other NASA centers (in particular with GSFC and MSC).

FIG. 23. JULY - AERIAL PHOTOGRAPHER'S CLEAR DAY MAP

VII. TERRAIN PHOTOGRAPHIC COVERAGE BY CAMERAS OF VARIOUS FOCAL LENGTHS

An understanding of the geometry included in this section is certainly not a prerequisite to developing an understanding of vertical photographic imagery of clouds which exists, i.e., which has already been obtained. A grasp of the basic geometric principles illustrated herein is, however, quite important and valuable to one charged with the responsibility of obtaining vertical photographic coverage of cloud structure or any other subject capable of being recorded photographically. Accordingly, this information has been included as a convenience to those involved in aerial photographic mission planning, whether for recording environmental phenomena, such as cloud structure, etc., or earth resources subjects.

Figure 24 shows some geometric relationships that exist between camera ground coverage "L", camera focal length "f", vertical height "H" of camera above the terrain, and the width "w" of the photograph's format.

The camera's perspective center is represented by the letter "o", the photograph's format is indicated by rectangle ABCD, and the terrain imaged in the resultant photograph is shown as rectangle EFGH. The camera's focal length represented by "f" is also known as the distance from the rear nodal point of the lens to the plane of infinite focus.

Lines JK and MP are parallel. By passing a plane through these lines and "o", the figure JKOMP is obtained, as shown at the right of Figure 24. Triangle JKO is similar to triangle OMP. Accordingly, one may say

$$\frac{\frac{L}{2}}{H} = \frac{\frac{w}{2}}{f}$$

by similar triangles, and since MP is one half the ground coverage or $\frac{L}{2}$, and JK is one-half the format width, or $\frac{w}{2}$. Solving this equation for L results in

$$L = \frac{wH}{f}$$

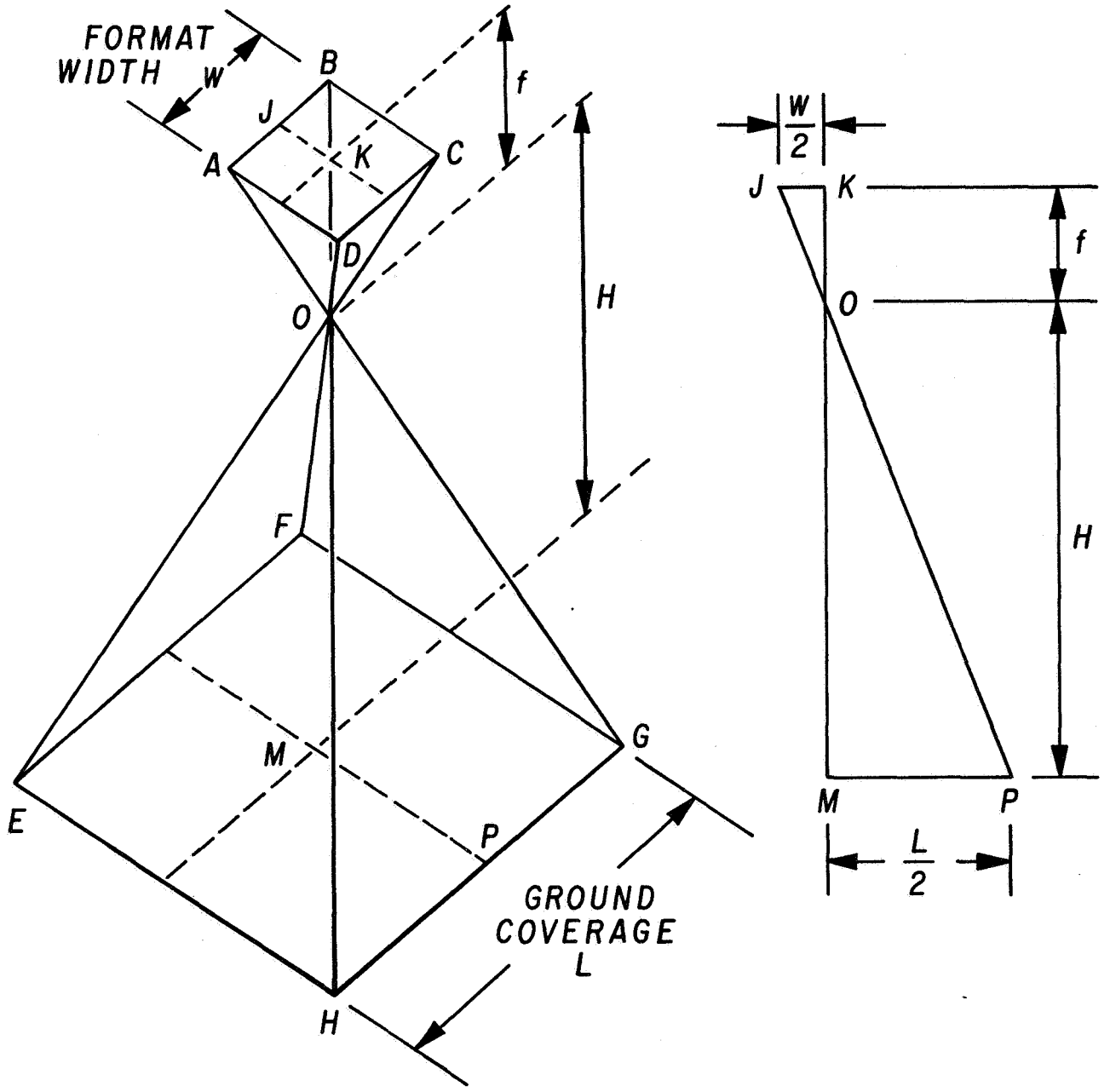

$$\frac{L/2}{H} = \frac{W/2}{f}$$

$$\therefore\ L = \frac{WH}{f}$$

FIG. 24. GROUND COVERAGE "L" IN TERMS OF FOCAL LENGTH "f", VERTICAL HEIGHT ABOVE TERRAIN "H", AND FORMAT WIDTH "w".

This relationship was then used to calculate the ground coverage for cameras with 9 in. × 9 in. (228.6 mm × 228.6 mm) formats, and with focal lengths of 3 in. (76.2 mm), 6 in. (152.4 mm), 12 in. (304.8 mm), and 24 in. (609.6 mm) at various assumed altitudes from 500 ft (152.4 m) to 1 000 000 ft (304, 800 m). These results are shown in Table 10.

A family of curves is shown in Figure 25, which was plotted from the values listed in Table 10. By knowing the altitude at which a camera will be operating, and by also knowing the focal length of its lens, one may easily determine the resultant ground coverage, from Figure 25. Or, if the ground coverage to be obtained photographically has been specified, then for a camera whose focal length is between 3 in. (76.2 mm) and 24 in. (609.6 mm), the flying height can be determined.

TABLE 10. GROUND COVERAGE IN FEET (METERS) FOR VARIOUS FOCAL LENGTH LENSES AND A 9 in. × 9 in. (228.6 mm × 228.6 mm) FORMAT

Height Above Terrain, H		Ground Coverage							
		3 in. (76.2 mm) Focal Length		6 in. (152.4 mm) Focal Length		12 in. (304.8 mm) Focal Length		24 in. (609.6 mm) Focal Length	
feet	meters	feet	meters	feet	meters	feet	meters	feet	meters
500	152.4	1 500	457.2	750	228.6	375	114.3	187.5	57.15
1 000	304.8	3 000	914.4	1 500	457.2	750	228.6	375	114.3
2 000	609.6	6 000	1 828.8	3 000	914.4	1 500	457.2	750	228.6
3 000	914.4	9 000	2 743.2	4 500	1 371.6	2 250	685.8	1 125	342.9
4 000	1 219.2	12 000	3 657.6	6 000	1 828.8	3 000	914.4	1 500	457.2
5 000	1 524.0	15 000	4 572.0	7 500	2 286.0	3 750	1 143.0	1 875	571.5
6 000	1 828.8	18 000	5 486.4	9 000	2 743.2	4 500	1 371.6	2 250	685.8
7 000	2 133.6	21 000	6 400.8	10 500	3 200.4	5 250	1 600.2	2 625	800.1
8 000	2 438.4	24 000	7 315.2	12 000	3 657.6	6 000	1 828.8	3 000	914.4
9 000	2 743.2	27 000	8 229.6	13 500	4 114.8	6 750	2 057.4	3 375	1 028.7
10 000	3 048.0	30 000	9 144.0	15 000	4 572.0	7 500	2 286.0	3 750	1 143.0
20 000	6 096.0	60 000	18 288.0	30 000	9 144.0	15 000	4 572.0	7 500	2 286.0
30 000	9 144.0	90 000	27 432.0	45 000	13 716.0	22 500	6 858.0	11 250	3 429.0
40 000	12 192.0	120 000	36 576.0	60 000	18 288.0	30 000	9 144.0	15 000	4 572.0
50 000	15 240.0	150 000	45 720.0	75 000	22 860.0	37 500	11 430.0	18 750	5 715.0
75 000	22 860.0	225 000	68 580.0	112 500	34 290.0	56 250	17 145.0	28 125	8 572.5
100 000	30 480.0	300 000	91 440.0	150 000	45 720.0	75 000	22 860.0	37 500	11 430.0
250 000	76 200.0	750 000	228 600.0	375 000	114 300.0	187 500	57 150.0	93 750	28 575.0
500 000	152 400.0	1 500 000	457 200.0	750 000	228 600.0	375 000	114 300.0	187 500	57 150.0
1 000 000	304 800.0	3 000 000	914 400.0	1 500 000	457 200.0	750 000	228 600.0	375 000	114 300.0

[THIS PAGE LEFT BLANK INTENTIONALLY]

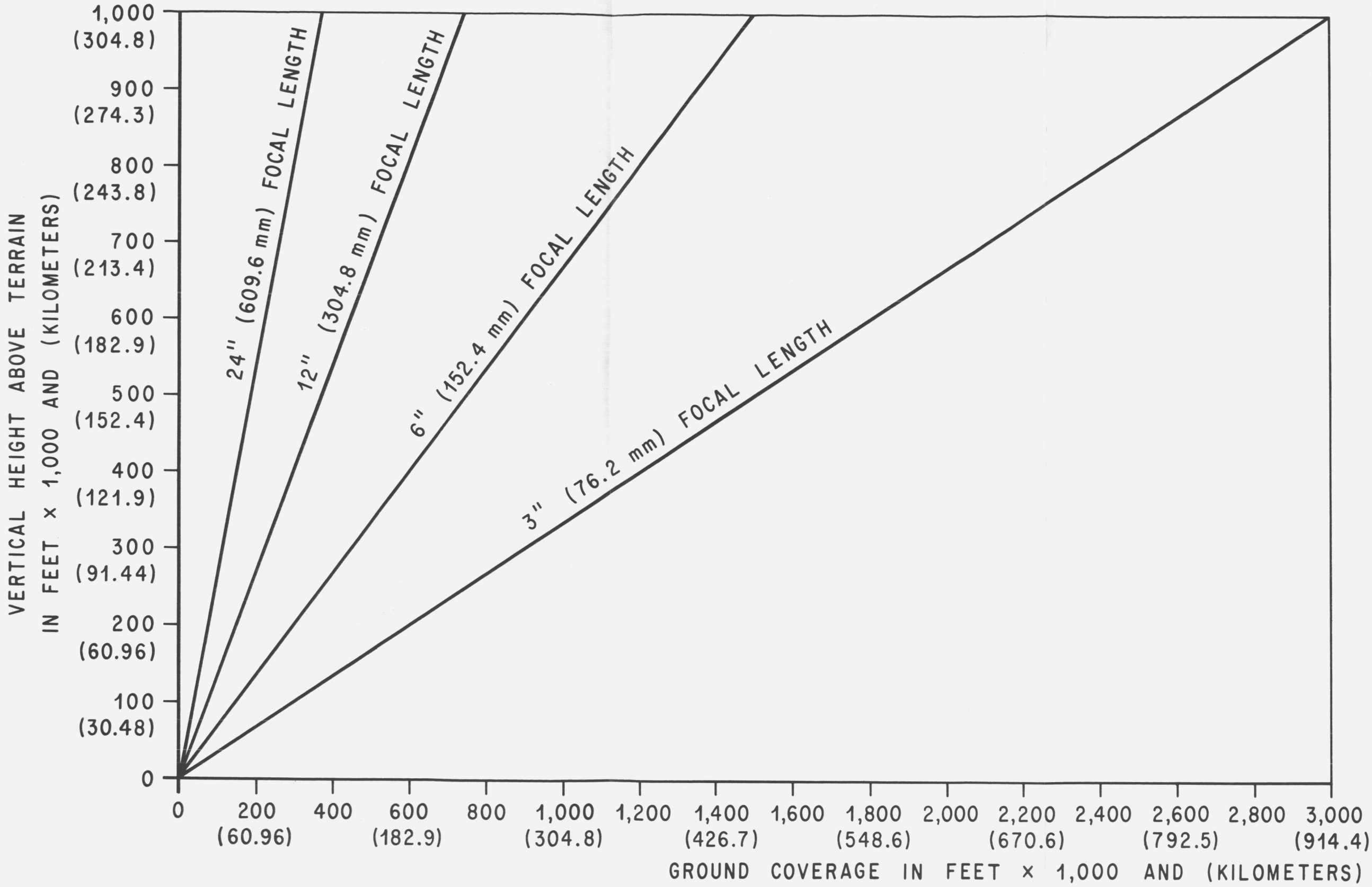

FIG. 25. GROUND COVERAGE VERSUS VERTICAL HEIGHT ABOVE TERRAIN FOR VARIOUS FOCAL LENGTHS AND A 9 in × 9 in (228.6 mm × 228.6 mm) FORMAT

VIII. CLOUD FORMATIONS AND OTHER DATA DERIVED FROM OBLIQUE ORBITAL PHOTOGRAPHS

In this section, two oblique photographs taken during the Apollo 9 mission are shown. A photo-interpretation for each photograph is provided, which discusses the various cloud formations recorded in them, as well as certain geographical highlights visible in the scenes. The first photograph to be discussed, AS 9-19-3047 (presented later in this section as Figure 27) is a high oblique photograph. A high oblique photograph is one which was taken with the camera's optical axis intentionally inclined to the vertical, and which contains the apparent horizon of the earth. The second photograph to be discussed, AS 9-19-3013 (presented later in this section as Figure 28) is a low oblique photograph. A low oblique photograph is one which was taken with the camera's axis intentionally inclined to the vertical, but upon which the apparent horizon of the earth does not appear.

When using oblique photographs for photogrammetric or photo-interpretation purposes, one must exercise caution when defining the photographic scale of any point on the imagery contained within the photograph. In conventional vertical photography, one can readily calculate the average photographic scale by knowing the camera's focal length, the altitude of the camera at the instant of exposure, and the average terrain elevation, or by knowing the distance between two visible photo-control points of equal elevation. However, in oblique photography, because of the attendant tilt of the camera's photographic axis, scale definition becomes somewhat more involved. One must first consider the "true horizon" of the oblique photograph, which is the photographic trace of a horizontal plane containing the exposure station. In Figure 26A, which shows some of the geometric relationships pertaining to an oblique photograph, the "true horizon" is the imaginary line defining the intersection of the horizontal plane (through the exposure station) with the plane of the photograph, and therefore does not appear on the photograph as a result of film exposure. Figure 26B shows the relationship of the "true horizon" to the "apparent horizon" on an oblique photograph. With these concepts in mind, it can be stated that there are two types of scale variation inherent in oblique photographs. The scale along the lines parallel to the true horizon is constant for any one line; and beginning at the true horizon, and working toward the bottom edge of the photograph, each succeeding line has a greater scale than does the previous one. Scale on these lines parallel to the true horizon is termed "x-scale." The scale of lines constructed perpendicular to the constant-scale lines, and parallel to the principal line, varies throughout their length. Scale on these lines parallel to the principal line is called "Y-scale." It is hoped that this brief discussion of scale variation on oblique photographs points out the necessity for exercising care when attempting to make measurements directly from oblique photographs.

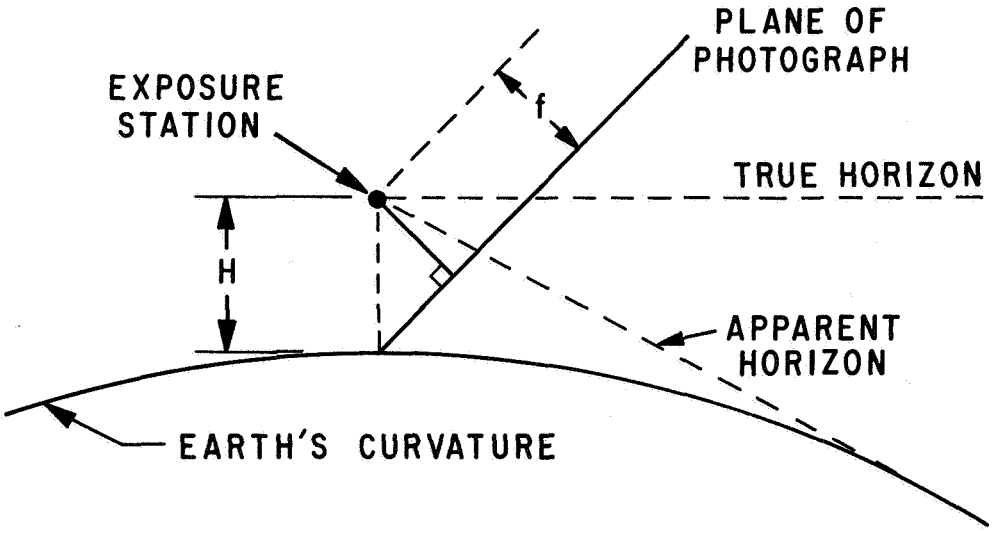

a) GEOMETRIC RELATIONSHIPS - OBLIQUE PHOTOGRAPHS

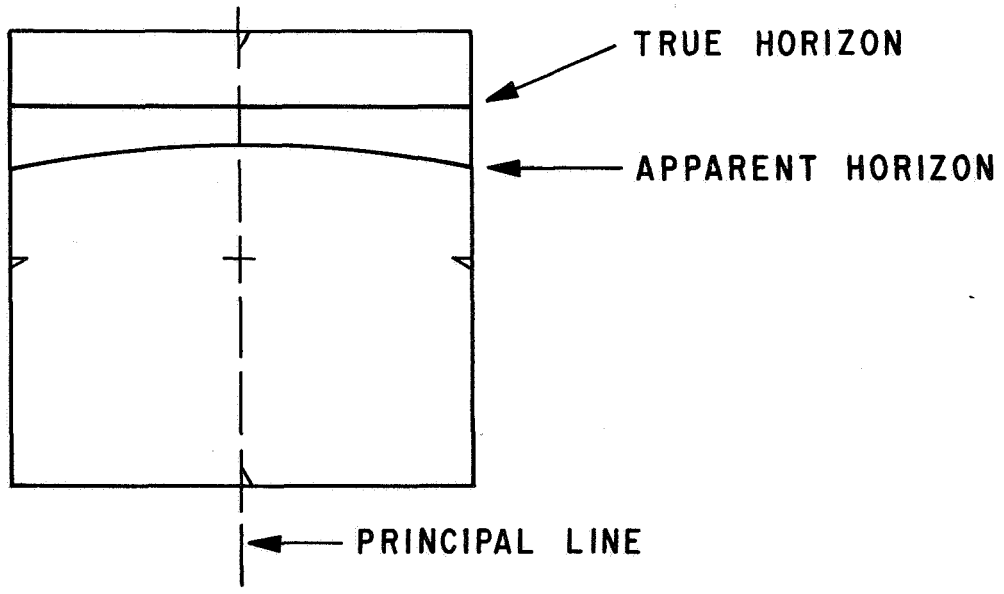

b) TRUE AND APPARENT HORIZONS ON AN OBLIQUE PHOTOGRAPH

60

FIG. 26.

Photo-Interpretation of Oblique Photograph AS 9-19-3047 (Fig. 27)

This high oblique photograph of the eastern coast of peninsular Florida, was taken March 10, 1969, at 17:42 hours Greenwich Mean Time (12:42 p.m. in the photograph's geographical location). The principal point is located at 27°45'N latitude, 80°26'W longitude, a point near Wabasso and Winter Beach, Florida. At the time of film exposure, the sun's elevation was 57 deg. The spacecraft's (camera's) altitude was 187 kilometers (101 nautical miles).

The view is approximately south-south easterly. Cloud formations, inland bodies of water and some geographical features which are readily identifiable are described in the following paragraphs.

At the time this high oblique photograph was taken, two prominent cloud formations were in evidence on the scene. The high clouds, stretching generally from west to east, in south Florida, appear to be of the cirrocumulus type. In the temperate regions these cirrocumulus clouds, which are considered to be in the "high" cloud family, generally occur from 5 to 13 kilometers altitude. Based upon the location of the shadow projected upon the peninsula by these clouds, the northern edge of the cloud structure appears to be over West Palm Beach on the east coast and crosses the state to Fort Myers on the west coast. "Mackerel sky" is a term used by sailors to describe cirrocumulus cloud formations whose groups or lines are uniformly arranged in the sky like ripples on the sands of a seashore.

The lower (altitude) cloud formation which extends from a few miles off the east coast, eastward out to sea beyond the area of coverage of the photograph's format, appears to be of the altocumulus type. Altocumulus clouds, in the temperate regions, generally occur from 2 to 7 kilometers in altitude; they are in the "middle cloud" family, and are composed of rather flattened globular masses or elements arranged in groups or lines or waves, and sometimes are sufficiently close that their edges appear to join. Altocumulus clouds may exist at several levels simultaneously and they are sometimes derived from decaying cumulus clouds.

The St. John's River, trending south-north parallel to the coastline, is visible in the lower left hand corner of the photograph. The city of Jacksonville is located at the point in the river where its south-to-north direction changes to easterly. Following the St. John's south to Palatka (inside crook in the river where it narrows down), one can see that it meanders into and out of

Lake George from the south. Lake George, as viewed in the direction presented in this photograph, looks somewhat like a head, with the nose pointed toward the east coast. Forty-six miles (74 km) due south from Lake George, Lake Apopka presents itself. Its area is slightly less than Lake George's. Lake Apopka is 68 miles (109 km) inland from Cape Kennedy, the prominent cape about half-way down the coastline from Jacksonville to the portion of south Florida which this day was covered by clouds. About 127 miles (204 km) south-south east from Lake Apopka, the large lake visible is Lake Okeechobee. The Kissimmee River, seen here as a light twisted line, feeds into Lake Okeechobee from the north-north west.

The cloud bank running parallel to the east coast is seaward sufficiently to permit a clear view of the Cape Kennedy area, although a few scattered clouds are seen over the area slightly south of the Cape Kennedy area. Starting from the north end of the prominent Cape Kennedy area, one sees three major strips of water, just inland from the coastline. The northernmost strip, which runs out along the Cape toward the south east, is known as Indian River Lagoon. Further down to the very tip of the cape, which is the Cape Kennedy Air Force Station, just inland can be seen the Banana River, trending due south. The largest water strip, which is more inland than the two previously discussed, is known as the Indian River. The Indian River continues southward inside of Jupiter Island, to the point where the St. Lucie Canal, from Lake Okeechobee, empties into the Atlantic Ocean. The Intra-Coastal Waterway is contained within the Indian River from a point north of Merrit Island at Cape Kennedy, to a point just south of St. Lucie Inlet.

Photo-Interpretation of Oblique Photograph AS 9-19-3013 (Fig. 28)

This low oblique photograph of a portion of Guerrero Province, on the southern coast of Mexico, was taken March 9, 1969, at 21:14 hours Greenwich Mean Time (3:15 p.m. in the photograph's geographical location). The principal point is located at 17° 58'N latitude, 98°45'W longitude, a point near Olinalá, in Guerrero Province. At the time of film exposure, the sun's elevation was 50 deg. Spacecraft's (camera's) altitude was 101 nautical miles (187 kilometers). The view is approximately south-south westerly. Cloud formations and various geographical features which can be identified in the photograph, are described in the following paragraphs.

The greyish or light blue looking areas that seem to emanate from points more or less in a band about 35 miles (56 km) inland from the coast, are smoke plumes. These probably are coming from forest fires in the mountainous area,

FIG. 27. HIGH OBLIQUE PHOTOGRAPH OF EASTERN FLORIDA TAKEN MARCH 10, 1969 FROM APOLLO 9 (AS 9-19-3047)

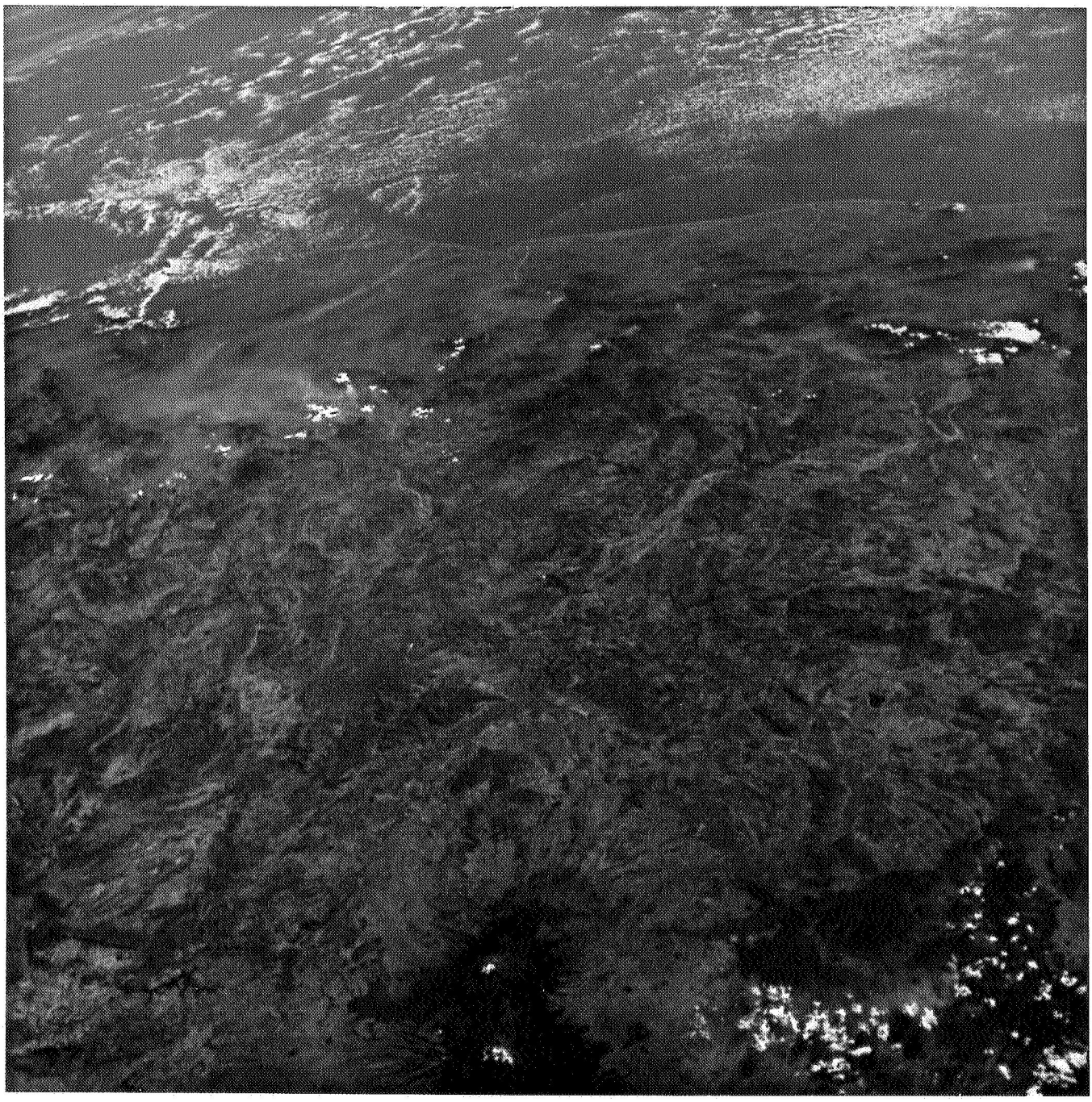

FIG. 28. LOW OBLIQUE PHOTOGRAPH OF SOUTHERN COAST OF MEXICO TAKEN MARCH 9, 1969 FROM APOLLO 9 (AS 9-19-3013)

since industrial polluters would not be in this extensive area because of the lack of roads in the vicinity, as determined from available maps of the area.

Some of the white patchy areas above the terrain part of the photograph are patches of snow and some are clouds. The patches over land in the upper right portion project shadows beneath them, so these shadows of course identify the patches as clouds. Over to the left of the photograph near the lower extremities of the densest plumes of smoke, one can observe several small white patches which are obviously under the lower left hand portion of the smoke cloud. It is quite likely that these are patches of snow on some of the higher elevations in that area. On the right end of this smoke plume, some clouds are visible above it. All along the area shown on the photograph, about 30 miles inland (48 km), the elevations of the prominent peaks range from about 8000 to 12 000 feet (2438 - 3658 m). So, it is quite likely that patches of snow accumulation could exist in that area. The few scattered clouds that are shown over the land appear to be of the type cumulus humilis since their vertical extent is not great with respect to the local terrain; in addition those clouds over land in the photograph's upper right, appear generally flattened. The high, scaly cloud formations out over the ocean are of the altocumulus variety.

Looking now at the Pacific coastline, the left hand border of the photograph intersects the coastline near Teotepec, a town about 15 miles (24 km) inland from the coast. Tracing now to the right along the coastline (in the direction of west-north west), and passing under the white cloud formations, one comes to a depression or notch in the coastline which is actually a large bay into which the "Rio Grande" empties (not the Rio Grande between Texas and Mexico). The river "Rio Grande" is visible as a faint tan line working east-south east from the bay, and then back to the north. Slightly to the east of the river, one can observe one of the many smokey areas of the photograph, which were discussed earlier. Tracing further north-west along the coastline from the bay, one passes two lagoons: Laguna Chantengo (first) and Laguna Tecomate (second). These are detectable as a lighter blue than the ocean. Next, the coastline is seen to jut out somewhat, and another river, the Papagayo, can be observed coming down out of the Sierra Madre del Sur (mountain range) to the point where it drains into the Pacific at still another lagoon, Laguna Papagayo.

The next prominent feature on the coastline, marked sharply by a well defined semi circular bay between Laguna Papagayo on the left and a small white patch on the right (possibly snow) is the famous Mexican resort city of Acapulco. For Acapulco, the average daily high temperature ranges from 89°F (31.7°C) in May, June, July and August to 85°F (29.4°C) in January.

The average daily low temperature ranges from 76°F (24.4°C) in June to 70°F (21.1°C) in December, January, February, and March. The rainiest month, on the average, in Acapulco is September with rain occurring on 18 days of the month. From November through May, there is very little, if any, recorded rainfall. One small lagoon is visible on the coast to the northwest of Acapulco, and the little river next visible to the northwest is the Coyuca.

Moving now to the center of the lower border of the photograph, snow peaked Mount Popocatepetl, a composite volcano, rises above the surrounding terrain. Popocatepetl's elevation is 17 887 feet (5451.9 m) above sea level. This steep sided cone was built by alternating lava outpourings and violent explosions that piled pyroclastic debris around the vent. Most composite volcanoes, such as Popocatepetl, Mount Rainier in Washington, Fujisan in Japan, and Mount Hood in Oregon, exhibit alternating fingers or rivulets of pyroclastic debris and tongues of lava, such as can be seen on this photograph. The main difference between composite volcanoes, such as Popocatepetl, and shield volcanoes such a Mauna Loa in the Hawaiian Islands, is in the strong explosive activity generally associated with composite volcanoes.

IX. SUMMARY REMARKS

Clouds and cloud shadows seriously degrade the value of orbital and aerial photographic imagery for photogrammetric and photo-interpretation purposes. Mission planners must take this into account before each launch. In the case of manned remote sensing platforms, such as Skylab, the astronauts should take into account the degrading effects of clouds and cloud shadows, when making real time decisions about when to operate experiment S-190, the Multispectral Photographic Facility, depending on the particular requirements of the test site to be imaged at the particular time.

It is recommended that future study effort in this area include the preparation of a controlled photo-mosaic, using, e.g., azimuth line control and suitably scaled vertical Apollo mission photographs which contain a reasonable percentage of cloud coverage over various parts of continental United States. This would allow a choice of several cloud covered areas, for study and atmospheric model testing, which were directly under measurable cloud structures and in which is located a National Weather Service station. A more realistic comparison of each ground based cloud observation with the photographically recorded cloud information above and around each corresponding ground observation point could then be made.

To simplify the measurement of the chosen cloud-covered areas, the use of a scanning microdensitometer or electric planimeter should be considered. The preparation of the controlled photo-mosaic will also increase the probability of being able to choose a cloud covered area for testing which was photographed at a time reasonably close to the time at which a WBAN reading was taken at the corresponding surface weather observation point.

Vertical orbital and aerial photographs which contain greater than 25 percent cloud coverage are of questionable value for most photogrammetric and photo-interpretation purposes.

Successful accomplishment of orbital and aerial photographic missions is greatly dependent upon four elements of our natural environment: clouds, haze, solar altitude, and turbulence (aerial missions only).

When considering the use of oblique orbital and aerial photographs for measurement purposes, one must exercise caution due to the "x" scale variation of lines parallel to the true horizon, and the "y" scale variation on lines parallel to the principal line.

REFERENCES

1. Sutcliffe, R. C.: Weather and Climate. The New American Library, Inc., February 1969.

2. Apollo 9 Photographic Plotting and Indexing Report (Including Aircraft Underflight). Prepared by Mapping Sciences Laboratory for Earth Resources Division, Science and Applications Directorate, Manned Spacecraft Center, Houston, Texas, October 1969.

3. Endlich, R. M.; Wolf, D. E.; Hall, D. J.; and Brain, A. E.: A Pattern Recognition Technique for Determining Cloud Motions from Sequences of Satellite Photographs. Prepared by Stanford Research Facility, Menlo Park, California, for Project Famos, Navy Weather Research Facility, Naval Air Systems Command, April 1970.

4. Brown, S. C.: Simulating the Consequence of Cloud Cover on Earth-Viewing Space Missions. Prepared by Aerospace Environment Division, Aero-Astrodynamics Laboratory, Marshall Space Flight Center, Alabama, for publication in the Bulletin of the American Meteorological Society, Vol. 51, No. 2, February, 1970, pp. 126-131.

APPROVAL

NASA TM X- 64710

PHOTOGRAMMETRY AND PHOTO-INTERPRETATION APPLIED TO ANALYSES OF CLOUD COVER, CLOUD TYPE, AND CLOUD MOTION

By Paul A. Larsen

The information in this report has been reviewed for security classification. Review of any information concerning Department of Defense or Atomic Energy Commission programs has been made by the MSFC Security Classification Officer. This report, in its entirety, has been determined to be unclassified.

This document has also been reviewed and approved for technical accuracy.

W. W. VAUGHAN
Chief, Aerospace Environment Division

E. D. GEISSLER
Director, Aero-Astrodynamics Laboratory

U.S. GOVERNMENT PRINTING OFFICE ☆ 1973 — 742-985